Mineral. Soc. Amer. Spec. Pap. **3**, 155–186 (1970).

A CHEMICAL AND THERMODYNAMIC MODEL OF ORE DEPOSITION IN HYDROTHERMAL SYSTEMS

HAROLD C. HELGESON

Department of Geology and Geophysics, University of California, Berkeley, California[1] *94720*

ABSTRACT

The major compositional characteristics of natural hydrothermal systems can be described in terms of 16 thermodynamic components; *e.g.*, NaCl-KCl-$MgCl_2$-$CaCl_2$-$FeCl_2$-CuCl-$ZnCl_2$-$PbCl_2$-AgCl-Al_2O_3-SiO_2-H_2S-H_2SO_4-HCl-H_2O-CO_2. The chemical potentials of approximately half of these components are commonly constant or functions of chemical equilibrium in hydrothermal processes. Many such processes involve relatively concentrated acid alkali-chloride solutions containing ppm concentrations of the ore-forming metals distributed predominantly in complexes with the chloride ion. Formation of hydrothermal ore deposits from such solutions is controlled by changes in temperature and/or pressure and chemical interaction of the aqueous phase with its mineralogic environment. Precipitation and replacement of sulfides and oxides in ore proportions may occur at constant temperature and pressure in response to increasing solution pH resulting from reaction of the aqueous phase with silicates and/or carbonates in the host rock to produce metasomatic mineral assemblages. The fugacities of O_2 and S_2 may increase or decrease in the process. A model of reversible and irreversible chemical reactions describing the process can be represented by a matrix of linear differential equations describing the change in the distribution of components among phases in the system as a function of the change in the composition of the aqueous phase resulting from reaction of the solution with its environment. Computer evaluation of the matrix equation together with thermodynamic calculations permits quantitative and simultaneous prediction of the mass transfer attending rock alteration and sulfide deposition in hydrothermal systems containing more than 60 components and chemical species. Thermodynamic data currently available permit calculations to be carried out for temperatures from 25° to 300°C. The calculations provide simultaneously for reversible and irreversible reactions, changes in the oxidation state of the system, variable activity coefficients, binary solid solutions, and equilibria among species in the aqueous phase and silicate, sulfide, oxide, carbonate, and sulfate minerals. Predicted quantities include the distribution of species in the aqueous phase at a function of reaction progress together with the mutual solubilities of minerals and the amounts precipitated and/or destroyed, the sequence in which they occur, and their cotectic-peritectic relations in either open or closed systems. The model affords close quantitative approximation of the actual chemical environment of rock alteration and ore deposition as well as the mass ratios, paragenesis, and zonal distribution of minerals commonly observed in ore deposits.

INTRODUCTION

Ore deposition is commonly associated with alteration of the country rock adjoining hydrothermal veins. The purpose of this communication is to define quantitatively the chemistry and mass transfer involved in the process responsible for this association at a given temperature and pressure; *i.e.*, isothermal-isobaric rock alteration and associated sulfide, oxide, sulfate, silicate, and carbonate deposition resulting from reaction of an aqueous vein solution with its mineralogic environment. The thermodynamic approach, principles, and data employed in the calculations are those summarized elsewhere in the general context of geochemical processes (Helgseon, 1967a, and b, 1968, 1969, 1970a; Helgeson and Garrels, 1968; Helgeson, Garrels, and Mackenzie, 1969; Helgeson, Brown and Leeper, 1969; Helgeson, Brown, Nigrini, and Jones, 1970—see also, Raymahashay and Holland, 1969).

Hydrothermal ore deposition, like mass transfer in all geochemical processes, is a path dependent function; *i.e.*, the mineral assemblages formed and the relative amounts of each mineral precipitated depend on the composition of the solution at each stage of reaction progress, and therefore on the previous reaction history of the solution with its environment (Helgeson, 1968; Helgeson, Garrels, and Mackenzie, 1969). For the most part hydrothermal reactions are incongruent, and they involve large numbers of components and phases. Reversible and irreversible reactions, metasomatic alteration of silicate and carbonate host rocks, diffusion of material to and from reaction fronts in the wall rock, bulk flow of the fluid in the fracture system, oxidation-reduction reactions, cotectic and peritectic precipitation of a wide variety of minerals, and changes in temperature and/or pressure are only a few of the many "processes" that occur simultaneously in natural hydrothermal systems. A statisfactory chemical model of ore deposition in these systems must provide for all such variables. At the same time it must account quantitatively for the mineral assemblages and paragenetic, zonal, and replacement features commonly observed in hydrothermal ore deposits. Part of the objective of the present contribution is to demonstrate that such a model can be constructed from thermodynamic relations and evaluated accurately with the aid of modern computers. First, however, we must establish the chemical characteristics of natural hydrothermal systems.

[1] The work reported here was carried out in the Department of Geological Sciences, Northwestern University, Evanston, Illinois.

RESUMÉ OF THE CHEMISTRY OF HYDROTHERMAL SYSTEMS

The major compositional characteristics of natural hydrothermal systems can be described in terms of approximately 16 thermodynamic components. Any one of several alternate sets of components consisting of individual elements, oxides, hydroxides, sulfides, and/or chlorides may be used to describe such systems, but a set consisting primarily of *actual* components (Thompson, 1959) of the aqueous phase is particularly well suited to description and interpretation of chemical potential constraints and the

TABLE 1. AQUEOUS EQUILIBRIA IN HYDROTHERMAL SOLUTIONS

$H_2O \rightleftharpoons H^+ + OH^-$	$PbCl^+ \rightleftharpoons Pb^{2+} + Cl^-$
$Al(OH)^{2+} \rightleftharpoons Al^{3+} + OH^-$	$PbCl_2 \rightleftharpoons Pb^{2+} + 2Cl^-$
$Al(OH)_4^- \rightleftharpoons Al^{3+} + 4OH^-$	$PbCl_3^- \rightleftharpoons Pb^{2+} + 3Cl^-$
$KCl \rightleftharpoons K^+ + Cl^-$	$PbCl_4^{2-} \rightleftharpoons Pb^{2+} + 4Cl^-$
$KSO_4^- \rightleftharpoons K^+ + SO_4^{2-}$	$ZnCl^+ \rightleftharpoons Zn^{2+} + Cl^-$
$NaCl \rightleftharpoons Na^+ + Cl^-$	$ZnCl_2 \rightleftharpoons Zn^{2+} + 2Cl^-$
$NaCO_3^- \rightleftharpoons Na^+ + CO_3^{2-}$	$ZnCl_3^- \rightleftharpoons Zn^{2+} + 3Cl^-$
$NaSO_4^- \rightleftharpoons Na^+ + SO_4^{2-}$	$ZnCl_4^{2-} \rightleftharpoons Zn^{2+} + 4Cl^-$
$CaCO_3 \rightleftharpoons Ca^{2+} + CO_3^{2-}$	$CuCl^+ \rightleftharpoons Cu^{2+} + Cl^-$
$CaHCO_3^+ \rightleftharpoons Ca^{2+} + H^+ + CO_3^{2-}$	$CuCl_2 \rightleftharpoons Cu^{2+} + 2Cl^-$
$CaSO_4 \rightleftharpoons Ca^{2+} + SO_4^{2-}$	$CuCl_3^- \rightleftharpoons Cu^{2+} + 3Cl^-$
$MgSO_4 \rightleftharpoons Mg^{2+} + SO_4^{2-}$	$CuCl_4^{2-} \rightleftharpoons Cu^{2+} + 4Cl^-$
$MgHCO_3^+ \rightleftharpoons Mg^{2+} + H^+ + CO_3^{2-}$	$H_4SiO_4 \rightleftharpoons H_3SiO_4^- + H^+$
$MgSO_4 \rightleftharpoons Mg^{2+} + SO_4^{2-}$	$HSO_4^- \rightleftharpoons H^+ + SO_4^{2-}$
$FeCl^{2+} \rightleftharpoons Fe^{3+} + Cl^-$	$HS^- \rightleftharpoons H^+ + S^{2-}$
$FeCl_2^+ \rightleftharpoons Fe^{3+} + 2Cl^-$	$H_2S \rightleftharpoons 2H^+ + S^{2-}$
$FeCl_3 \rightleftharpoons Fe^{3+} + 3Cl^-$	$HCO_3^- \rightleftharpoons H^+ + CO_3^{2-}$
$FeCl_4^- \rightleftharpoons Fe^{3+} + 4Cl^-$	$H_2CO_3 \rightleftharpoons 2H^+ + CO_3^{2-}$
$CuCl_2^- \rightleftharpoons Cu^+ + 2Cl^-$	$HCl \rightleftharpoons H^+ + Cl^-$
$CuCl_3^{2-} \rightleftharpoons Cu^+ + 3Cl^-$	$MgOH^+ \rightleftharpoons Mg^{2+} + OH^-$
$8Cu^{2+} + 4H_2O + S^{2-} \rightleftharpoons 8Cu^+ + SO_4^{2-} + 8H^+$	$FeOH^+ \rightleftharpoons Fe^{2+} + OH^-$
	$CaOH^+ \rightleftharpoons Ca^{2+} + OH^-$
$8Fe^{3+} + 4H_2O + S^{2-} \rightleftharpoons 8Fe^{2+} + SO_4^{2-} + 8H^+$	$FeOH^{2+} \rightleftharpoons Fe^{3+} + OH^-$

chemistry of mass transfer in hydrothermal processes (Helgeson, 1970a). One such set of components consists of NaCl-KCl-$MgCl_2$-$CaCl_2$-$FeCl_2$-CuCl-$ZnCl_2$-PbCl-AgCl-HCl-H_2S-H_2SO_4-H_2O-CO_2-Al_2O_3-SiO_2. The compositions of most silicate, carbonate, sulfide, sulfate, and oxide minerals in hydrothermal systems can be expressed arithmetically in terms of these components, but in most cases both addition and subtraction of components is required. Consequently, mineral compositions are better expressed diagrammatically in terms of elemental, oxide, and/or sulfide components.

Thermodynamic components are distributed among a large number of chemical species in hydrothermal solutions. Where homogeneous equilibrium prevails in the aqueous phase the relation of the activities of the more abundant of these species and components to one another can be described by the reversible chemical reactions shown in Table 1. The reactions given in the table include chemical species that may be present in significant concentrations in "acid" chloride-rich hydrothermal solutions in the temperature range, 25°–300°C (Helgeson, 1969). Fluid inclusion data (*e.g.*, see Roedder, 1967) suggest that hydrothermal solutions involved in the formation of ore deposits commonly contain large concentrations of NaCl and/or $CaCl_2$, and to a lesser extent KCl and CO_2. "Typical" ore-forming solutions probably have compositional characteristics like those in Table 2.

TABLE 2. APPROXIMATE COMPOSITION OF HYDROTHERMAL ORE-FORMING SOLUTIONS

Component	Total Molality[a]
NaCl	0.01 to >3.0
KCl	<0.5
$CaCl_2$	0.01 to >3.0
$MgCl_2$	0.001[b]
$FeCl_2$	0.001[b]
CuCl	0.001[b]
$ZnCl_2$	0.001[b]
$PbCl_2$	0.001[b]
AgCl	0.001[b]
HCl	<0.1
H_2S	<0.1
H_2SO_4	<0.1
CO_2	<0.1
Al_2O_3	<0.1
SiO_2	<0.01

[a] Estimated from fluid inclusion data (c.f., Roedder, 1967) and thermodynamic considerations (Barton, 1959; Helgeson, 1964, 1967a and b, 1969).

[b] Order of magnitude.

Experimental solubility studies of rock alteration mineral assemblages (*e.g.*, see Hemley and Jones, 1964) and thermodynamic calculations (Helgeson, 1967a, 1969) suggest that the activity of the hydrogen ion in hydrothermal solutions is commonly of the order of 10^{-2} to 10^{-5} at elevated temperatures. This observation is based on the pH requirement for equilibrium among alteration minerals such as kaolinite and montmorillonite (or K-mica) and hydrothermal solutions in which m_{NaCl}, m_{CaCl_2}, and/or m_{KCl} are of the order of one or more. Recent experimental investigation of the stability of alunite in hydrothermal systems (Hemley, Hostetler, Gude, and Mountjoy, 1969) leaves little doubt that the pH of some hydrothermal solutions is even less than 2 at high temperatures.

Carbonates in hydrothermal systems are compatible with acid CO_2-rich aqueous solutions. This observation is illustrated in Figure 1 by the iso-pH curves representing

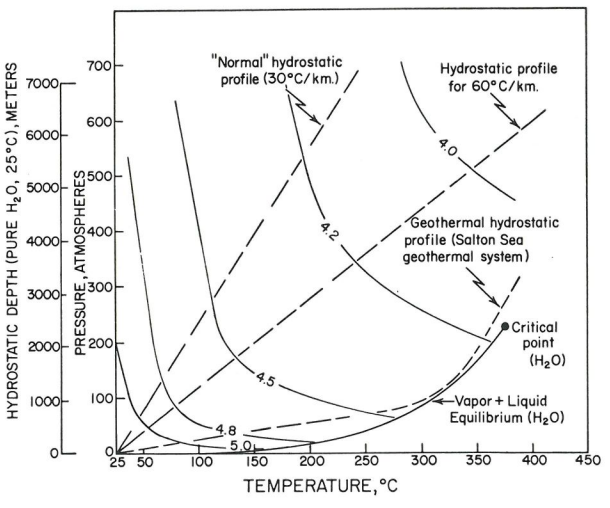

FIG. 1. Pressure-temperature diagram depicting iso-pH curves for equilibrium between calcite and an aqueous phase in which $a_{Ca^{2+}} = 0.01$ for the limiting case of unit activity of H_2O and $P_{CO_2} = P_{hydrostatic}$ ($CaCO_{3(c)} + 2H^+ \rightleftharpoons Ca^{2+} + CO_{2(g)} + H_2O_{(l)}$). The fugacity coefficients used in the calculations were computed from the reduced pressure and temperature chart reproduced by Garrels and Christ (1965); all of the other thermodynamic data were taken from Helgeson (1969).

TABLE 3. REVERSIBLE REACTIONS DESCRIBING EQUILIBRIA BETWEEN MINERALS AND THE AQUEOUS PHASE IN HYDROTHERMAL SYSTEMS

Native copper
$8Cu+8H^+ + SO_4^{2-} \rightleftharpoons 8Cu^+ + 4H_2O + S^{2-}$
Pyrrhotite
$FeS \rightleftharpoons Fe^{2+} + S^{2-}$
Sphalerite, Wurzite
$ZnS \rightleftharpoons Zn^{2+} + S^{2-}$
Galena
$PbS \rightleftharpoons Pb^{2+} + S^{2-}$
Covellite
$CuS \rightleftharpoons Cu^{2+} + S^{2-}$
Acanthite
$Ag_2S \rightleftharpoons 2Ag^{2+} + S^{2-}$
Chalcocite
$Cu_2S \rightleftharpoons 2Cu^+ + S^{2-}$
Pyrite
$FeS_2 + H_2O \rightleftharpoons Fe^{2+} + 1.75S^{2-} + 0.25SO_4^{2-} + 2H^+$
Chalcopyrite
$CuFeS_2 \rightleftharpoons Cu^{2+} + Fe^{2+} + 2S^{2-}$
Bornite
$Cu_5FeS_4 \rightleftharpoons 4Cu^+ + Cu^{2+} + Fe^{2+} + 4S^{2-}$
Cuprite
$Cu_2O + 2H^+ \rightleftharpoons 2Cu^+ + H_2O$
Magnetite
$Fe_3O_4 + 8H^+ \rightleftharpoons Fe^{2+} + 2Fe^{3+} + 4H_2O$
Hematite
$Fe_2O_3 + 6H^+ \rightleftharpoons 2Fe^{3+} + 3H_2O$
Brucite
$Mg(OH)_2 \rightleftharpoons Mg^{2+} + 2OH^-$
Gibbsite
$Al(OH)_3 \rightleftharpoons Al^{3+} + 3OH^-$
Calcite
$CaCO_3 \rightleftharpoons Ca^{2+} + CO_3^{2-}$
Anglesite
$PbSO_4 \rightleftharpoons Pb^{2+} + SO_4^{2-}$
Cerrusite
$PbCO_3 \rightleftharpoons Pb^{2+} + CO_3^{2-}$
Tenorite
$CuO + 2H^+ \rightleftharpoons Cu^{2+} + H_2O$
Smithsonite
$ZnCO_3 \rightleftharpoons Zn^{2+} + CO_3^{2-}$
Siderite
$FeCO_3 \rightleftharpoons Fe^{2+} + CO_3^{2-}$
Dolomite
$CaMg(CO_3)_2 \rightleftharpoons Ca^{2+} + Mg^{2+} + 2CO_3^{2-}$
Anhydrite
$CaSO_4 \rightleftharpoons Ca^{2+} + SO_4^{2-}$
Gypsum
$CaSO_4 \cdot 2H_2O \rightleftharpoons Ca^{2+} + SO_4^{2-} + 2H_2O$
Quartz
$SiO_2 + 2H_2O \rightleftharpoons H_4SiO_4$
Microcline
$KAlSi_3O_8 + 4H^+ + 4H_2O \rightleftharpoons K^+ + 3H_4SiO_4 + Al^{3+}$
Low Albite
$NaAlSi_3O_8 + 4H^+ + 4H_2O \rightleftharpoons Na^+ + 3H_4SiO_4 + Al^{3+}$
Anorthite
$CaAl_2Si_2O_8 + 8H^+ \rightleftharpoons Ca^{2+} + 2Al^{3+} + 2H_4SiO_4$
Leucite
$KAlSi_2O_6 + 2H_2O + 4H^+ \rightleftharpoons K^+ + Al^{3+} + 2H_4SiO_4$
Nepheline
$NaAlSiO_4 + 4H^+ \rightleftharpoons Na^+ + Al^{3+} + H_4SiO_4$
Analcite
$NaAlSi_2O_6 \cdot H_2O + H_2O + 4H^+ \rightleftharpoons Na^+ + Al^{3+} + 2H_4SiO_4$
Kaolinite
$Al_2Si_2O_5(OH)_4 + 6H^+ \rightleftharpoons H_2O + 2Al^{3+} + 2H_4SiO_4$

Na-Montmorillonite
$Na_{0.333}Al_{2.333}Si_{3.667}O_{10}(OH)_2 + 7.332H^+ + 2.668H_2O \rightleftharpoons 0.333Na^+ + 2.333Al^{3+} + 3.667H_4SiO_4$
K-Montmorillonite
$K_{0.333}Al_{2.333}Si_{3.667}O_{10}(OH)_2 + 7.332H^+ + 2.668H_2O \rightleftharpoons 0.333Na^+ + 2.333Al^{3+} + 3.667H_4SiO_4$
Ca-Montmorillonite
$Ca_{0.1665}Al_{2.333}Si_{3.667}O_{10}(OH)_2 + 7.332H^+ + 2.668H_2O \rightleftharpoons 0.1665Ca^{2+} + 2.333Al^{3+} + 3.667H_4SiO_4$
Mg-Montmorillonite
$Mg_{0.1665}Al_{2.333}Si_{3.667}O_{10}(OH)_2 + 7.332H^+ + 2.668H_2O \rightleftharpoons 0.1665Mg^{2+} + 2.333Al^{3+} + 3.667H_4SiO_4$
Muscovite
$KAl_3Si_3O_{10}(OH)_2 + 10H^+ \rightleftharpoons K^+ + 3Al^{3+} + 3H_4SiO_4$
Illite
$K_{0.6}Mg_{0.25}Al_{2.30}Si_{3.50}O_{10}(OH)_2 + 8H^+ + 2H_2O \rightleftharpoons 0.6K^+ + 0.25Mg^{2+} + 2.30Al^{3+} + 3.5H_4SiO_4$
Biotite (Annite)
$KFe_3AlSi_3O_{10}(OH)_2 + 10H^+ \rightleftharpoons K^+ 3Fe^{2+} + Al^{3+} + 3H_4SiO_4$

equilibrium between calcite and a solution in which $a_{Ca}{}^{++}=0.01$ for the limiting case of $P_{CO_2}=P_{\text{hydrostatic}}$. It can be deduced from Figure 1 that calcite may be present in hydrothermal systems involving a concentrated calcium chloride solution with a pH lower than 4 at elevated temperatures and pressures. Similar calculations indicate that other carbonates (such as siderite) may coexist with an aqueous solution having even a lower pH under comparable conditions. In contrast, it can be shown that "neutral" *p*H varies from 7.0 at 25° to 6.13 at 100°, 5.63 at 200° and 5.51 at 300°C (Fisher, 1969).

The distribution of thermodynamic components among phases in equilibrium models of hydrothermal systems can be represented by reversible reactions between minerals and the aqueous phase such as those shown in Table 3. Equilibrium constants for the reactions shown in Tables 1 and 3 have been summarized elsewhere (Helgeson, 1969) for 0°, 25°, 60°, 100°, 150°, 200°, 250°, and 300°C. These data permit diagrammatic representation of hydrothermal equilibria in terms of the activities of species in the aqueous phase.

DESCRIPTION OF PHASE RELATIONS

Phase relations among hydrothermal minerals are commonly described solely in terms of their compositions or the fugacities of oxide, sulfide, and/or elemental components. In "dry" sulfide-oxide systems, the fugacities of S_2 and O_2 are useful descriptive variables because they can

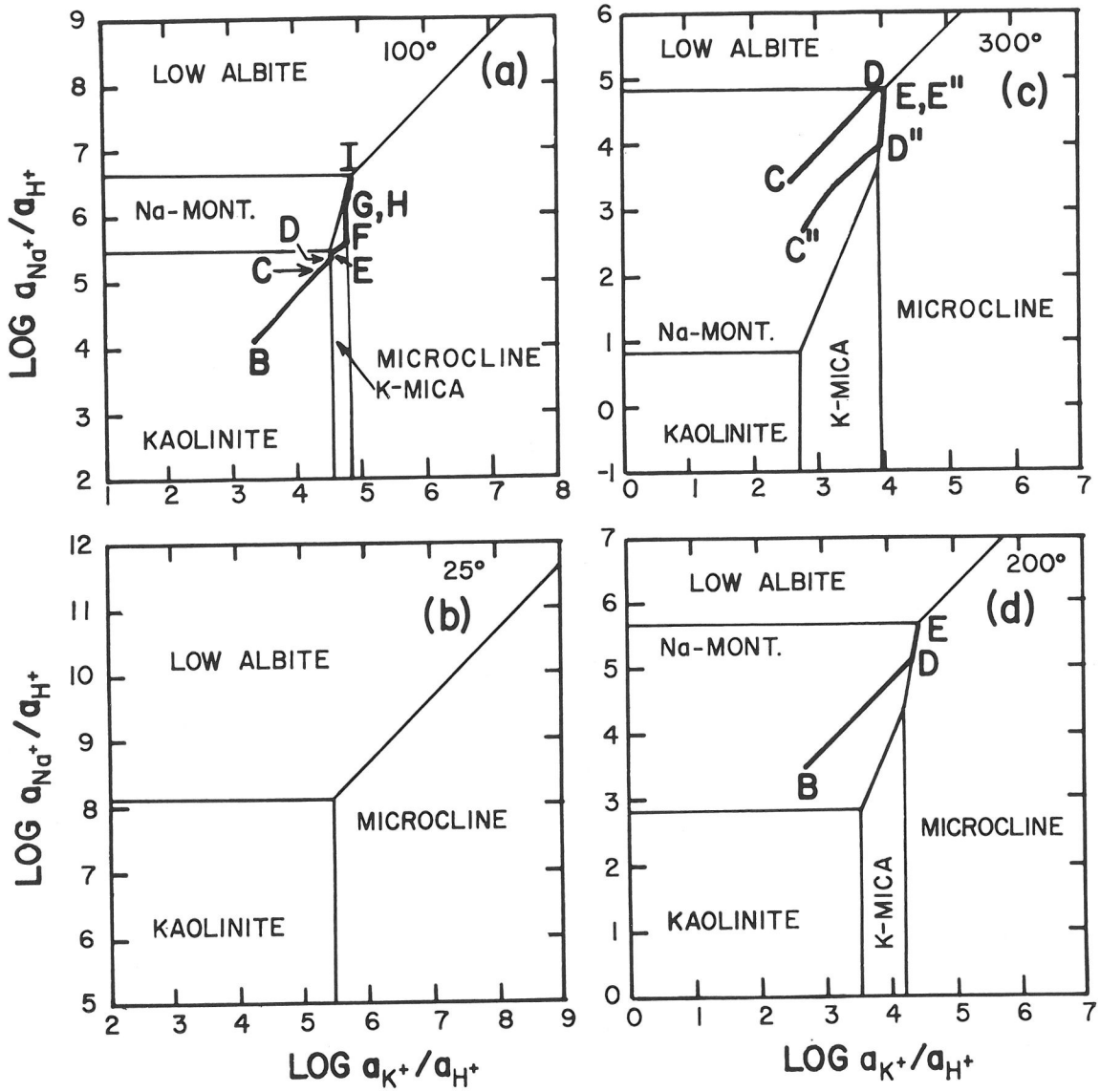

FIG. 2. Theoretical activity diagrams for the system KCl-NaCl-HCl-Al_2O_3-SiO_2-H_2O in the presence of quartz and an aqueous phase at one atmosphere, unit activity of H_2O, and 25° (b), 100° (a), 200° (d), and 300° (c) C. The heavy black lines and letter annotations refer to reactions discussed in the text. The thermodynamic data used to construct the diagrams were taken from Helgeson (1969).

be measured readily. In contrast, where hydrothermal solutions are involved these variables are commonly small in magnitude and not easily measured. In such systems, compositional parameters such as the activities of cations present (in the aqueous phase) in readily detectable concentrations are particularly useful variables for describing mineral equilibria.

The activity of a thermodynamic component can be represented in terms of ion activities in the aqueous phase by first writing the general relation,

$$M_{\nu_+}L_{\nu_-} + \nu_+ Z_+ H^+ \rightleftharpoons \nu_+ M^{Z_+} + \nu_- H_Z - L \qquad (1)$$

for which

$$\frac{a_{M^{Z_+}}^{\nu_+} a_{H_{Z_-}L}^{\nu_-}}{a_{M_{\nu_+}L_{\nu_-}} a_{H^+}^{\nu_+ Z_+}} = K_1 \qquad (2)$$

where ν_+ and ν_- stand for the number of moles of the cation (M) and anion (L), respectively, in one mole to the component represented by $M_{\nu_+}L_{\nu_-}$, H refers to hydrogen, Z_+ and Z_- are the charges on the cation and anion in the component, $a_{M^{Z+}}$ represents the activity of the subscripted species, and K_1 is the equilibrium constant for reaction (1). The relation between the change in the chemical potential of a component and its activity during a geochemical process is given by Helgeson (1970a).

$$\frac{d\mu_{M_{\nu+}L_{\nu-}}}{d\xi} = \frac{RT\, d\ln a_{M_{\nu+}L_{\nu-}}}{d\xi}$$
$$= \frac{\nu_+ RT\, d\ln a_M{}^{z+}/a_{H^+}{}^{Z_+}}{d\xi} + \frac{\nu_- RT\, d\ln a_{H_{Z-}L}}{d\xi} \quad (3)$$

where ξ is the progress variable for the process (De Donder, 1920; Prigogine and Defay, 1954; Helgeson, 1968).

It can be deduced from Equation (3) that all equilibria in hydrothermal systems can be represented in terms of the ratios of the activities of cations in the aqueous phase to that of the hydrogen ion. To illustrate this observation, a number of equilibria are portrayed in these terms in Figures 2–9. The diagrams in these figures have several advantages over their fugacity counterparts (*e.g.*, Fig. 10). The most important of these is the fact that the ordinate and abscissa can be interpreted directly and quantitatively in terms of the analytical concentrations of actual thermodynamic components in hydrothermal solutions (*e.g.*, see Helgeson, 1969, 1970a, and Fig. 9); mutual solubilities of minerals can therefore be computed conveniently from the diagrams. Also, silicate, carbonate, oxide, sulfate, and sulfide equilibria can be represented in terms of the same variables in a single diagram (*e.g.*, see Helgeson, Brown, and Leeper, 1969, and Fig. 4).

It has been demonstrated (*e.g.*, Helgeson, 1967a; Helgeson, Garrels, and Mackenzie, 1969; Ellis and Mahon, 1967; Althaus and Johannes, 1969) that the order of magnitude of the mass transfer of alkali and alkaline earth components (or cations corresponding to components) to or from the aqueous phase in hydrothermal reactions is commonly much smaller than the total concentrations of these components in solution (*i.e.*, $dm_i/d\xi \ll m_i$ where m_i refers to the total molality of the ith component in solution). This is particularly true for NaCl and/or $CaCl_2$, which are usually present in relatively large concentrations in hydrothermal solutions (Roedder, 1967). The chemical potentials of such components remain constant during reaction progress, which imposes constraints on the identities and amounts of phases made and destroyed as the solution reacts with its environment (Helgeson, 1970a).

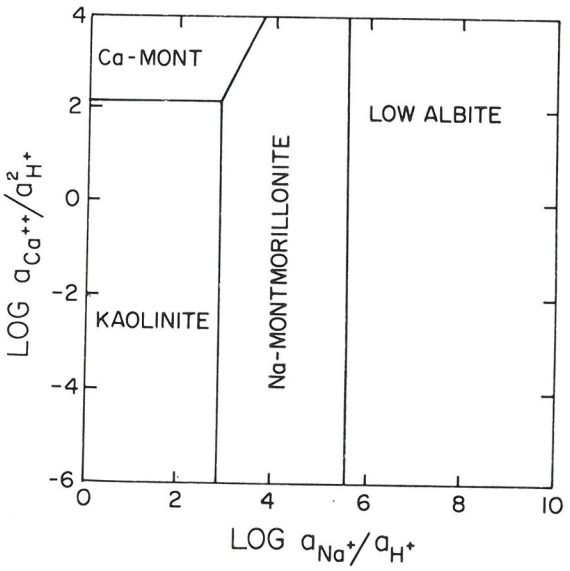

FIG. 3. Abridged theoretical activity diagram for the system $CaCl_2$-NaCl-HCl-Al_2O_3-SiO_2-H_2O in the presence of quartz and an aqueous phase at 200°C, one atmosphere, and unit activity of H_2O (Helgeson, Brown, and Leeper, 1969—reproduced with permission from Freeman, Cooper and Co.).

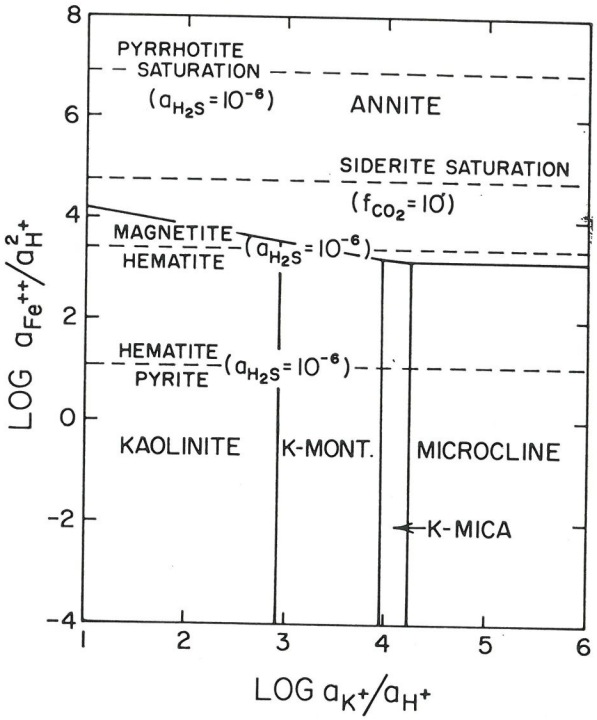

FIG. 4. Abridged theoretical activity diagram for the system $FeCl_2$-KCl-HCl-Al_2O_3-SiO_2-H_2S-H_2SO_4-CO_2-H_2O in the presence of quartz and an aqueous phase at 200°C, one atmosphere, and unit activity of H_2O (Helgeson, Brown, and Leeper, 1969—reproduced with permission from Freeman, Cooper and Co.).

CHEMICAL REACTIONS AND MASS TRANSFER

Let us consider the extent to which the chemistry of a solution changes as it reacts with its environment while passing through a fracture in a rock with which it is not in equilibrium. If we specify constant temperature and pressure and describe progress in all chemical reactions in terms of the hypothetical variable, ξ, we need make no explicit provision in our model calculations for reaction kinetics (Helgeson, 1970b and c), mechanisms of mass transfer, or the actual spatial and temporal (except to say that the derivative of ξ with respect to time is always positive) distribution of reaction products (Helgeson, 1968). Nevertheless, we can ask such questions as

1. What sequence of chemical events occurs during the reaction process?

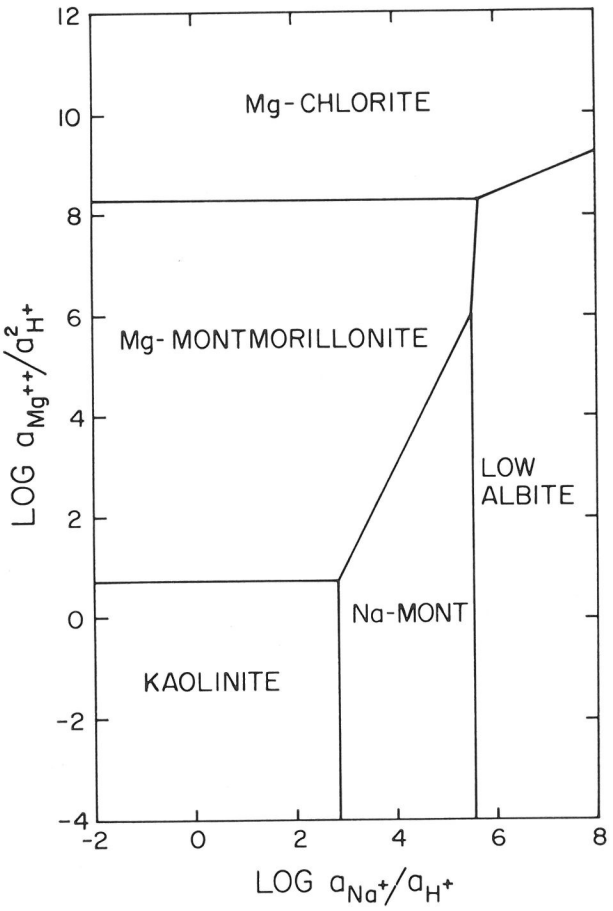

FIG. 5. Abridged theoretical activity diagram for the system $MgCl_2$-NaCl-HCl-Al_2O_3-SiO_2-H_2O in the presence of quartz and an aqueous phase at 200°C, one atmosphere, and unit activity of H_2O (Helgeson, Brown, and Leeper, 1969—reproduced with permission from Freeman, Cooper and Co.).

2. How much of the various reaction products are made and destroyed (kgm H_2O)$^{-1}$?
3. Does the chemical and thermodynamic model adequately account for the chemical and mineralogic characteristics of ore deposits?

Answers to these questions can be obtained by specifying the initial composition of the system and evaluating an array of differential thermodynamic equations describing equilibrium and mass transfer among species involved in the reaction process (Helgeson, 1968; Helgeson, Garrels, and Mackenzie, 1969; Helgeson, Brown, Nigrini, and Jones, 1970).

Thermodynamic relations. The extent to which minerals are produced and/or destroyed as a hydrothermal solution reacts with its mineralogic environment can be predicted by simultaneous evaluation of linear differential equations describing the conservation of mass, conservation of charge, and reversible mass transfer in the system. For isobaric-isothermal processes involving minerals of fixed composition and an aqueous phase in which the activity of H_2O is constant (discussed below), these equations can be expressed as (Helgeson, 1968)

$$\sum_j \nu_{i,j}\bar{n}_j + \sum_\phi \nu_{i,\phi}\bar{n}_\phi = 0, \tag{4}$$

$$\sum_j Z_j\bar{n}_j = 0, \tag{5}$$

and

$$\sum_j \frac{\hat{n}_{j,l}\bar{n}_j}{m_j} = -\sum_j \hat{n}_{j,l}\frac{d\ln\gamma_j}{d\xi} \tag{6}$$

where $\nu_{i,j}$ and $\nu_{i,\phi}$ refer to the number of moles of the ith element in the jth aqueous species and ϕth mineral, respectively, Z_j is the charge on the subscripted species, $\hat{n}_{j,l}$ is the coefficient of the jth aqueous species in the lth reversible reaction, m_j and γ_j are the molality and activity coefficients, respectively, of the subscripted species, and $\bar{n}_j$ and $\bar{n}_\phi$ are the reaction coefficients (kgm H_2O)$^{-1}$ of the jth species and ϕth mineral in the irreversible reaction. The latter variables are defined by (Helgeson, 1968)

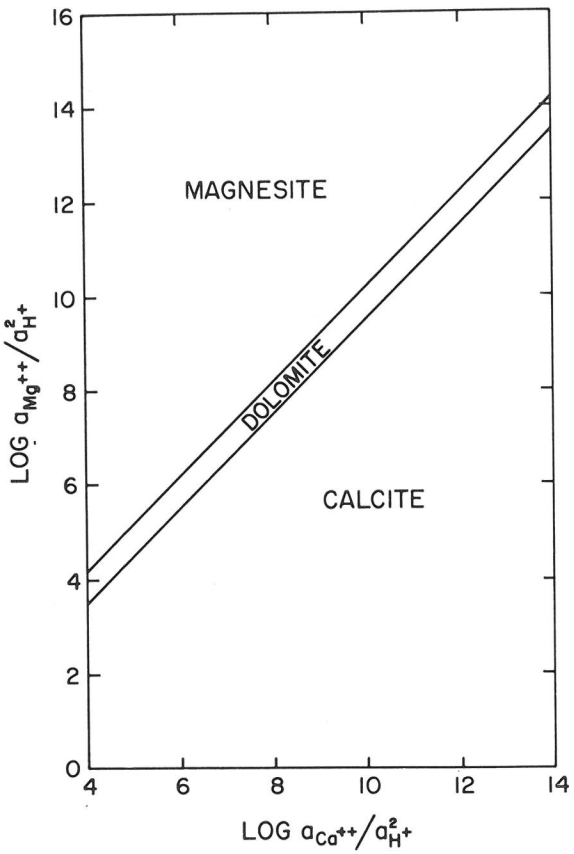

FIG. 6. Abridged theoretical activity diagram for the system $MgCl_2$-$CaCl_2$-HCl-CO_2-H_2O at 200°C, one atmosphere, and unit activity of H_2O (Helgeson, Brown and Leeper, 1969—reproduced with permission from Freeman, Cooper and Co.).

$$\bar{n}_j = \frac{dm_j}{d\xi} \tag{7}$$

and

$$\bar{n}_\phi = \frac{d\bar{x}_\phi}{d\xi} \tag{8}$$

where ξ is again the progress variable for the overall irreversible reaction and $\bar{x}_\phi$ refers to the number of moles (kgm H_2O)$^{-1}$ of the ϕth reactant or product mineral in the system. The reaction coefficients, $\hat{n}_j$, $\bar{n}_j$, and $\bar{n}_\phi$ are positive for products and negative for reactants.

The calculations reported below are based in part on the assumption that, (1) homogeneous equilibrium prevails in the system, (2) no mass is exchanged between the system and its surroundings, (3) no supersaturation occurs in the aqueous phase, and (4) the activity of H_2O can be regarded as unity (which is true in most instances; Helgeson, 1969). Under these conditions, expressions of Equation (4) can be written for each element in the system described by the 16 components listed above. In addition, we can write statements of Equation (6) for each reversible reaction in Table 1, and those in Table 3 for the minerals

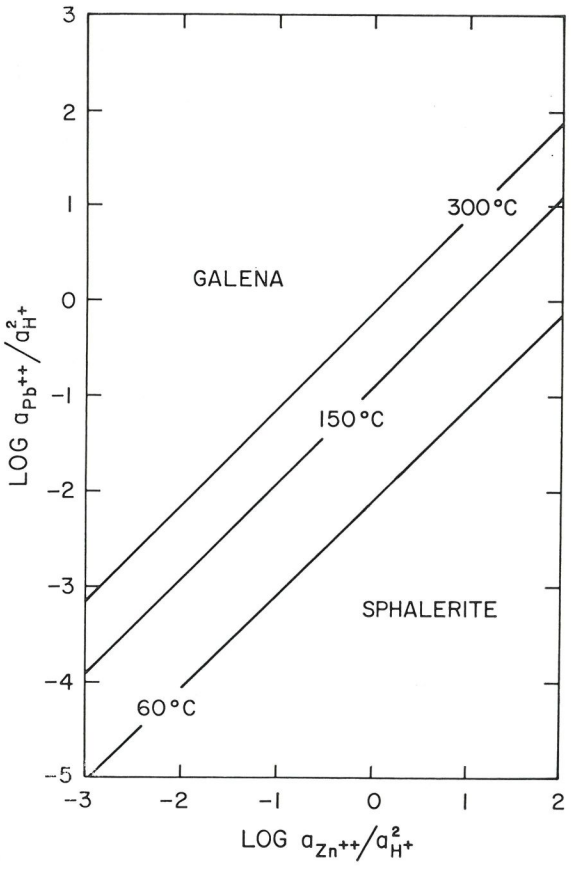

FIG. 7. Abridged theoretical activity diagram for the system $PbCl_2$-$ZnCl_2$-HCl-H_2S-H_2O at one atmosphere, unit activity of H_2O, and 60°, 150°, and 300°C, calculated from thermodynamic data taken from Helgeson (1969).

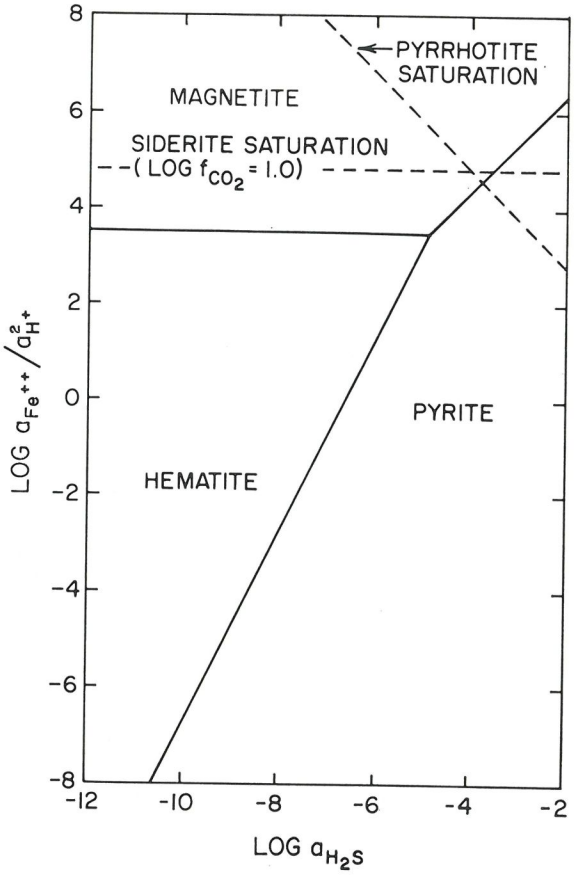

FIG. 8. Abridged theoretical activity diagram for the system $FeCl_2$-HCl-H_2S-H_2SO_4-CO_2-H_2O at 200°C, one atmosphere, and unit activity of H_2O (Helgeson, Brown, and Leeper, 1969—reproduced with permission from Freeman, Cooper and Co.).

with which the solution is saturated. These equations, together with Equation (5) constitute an array of linear differential equations in which the number of unknown reaction coefficients is equal to or less than the number of equations (Helgeson, 1968). Modification of these equations can be made to include provision for solid solution and the effect of changing activity of H_2O and/or activity coefficients on reaction progress (Helgeson, Brown, Nigrini, and Jones, 1970). For a given initial reactant mineral assemblage and solution composition, the array of equations can be solved quickly using matrix algebra and a high speed digital computer. The resulting values of $\bar{n}_j$ and $\bar{n}_\phi$ can then be used to predict the distribution of components in the system after a given increment of reaction progress. Taylor's expansions (truncated after the quadratic term) are suitable for this purpose (Helgeson, 1968); *i.e.*,

$$m_j = m_j^0 + \bar{n}_j \Delta\xi + \frac{\bar{n}_j' (\Delta\xi)^2}{2!} + \cdots \tag{9}$$

and

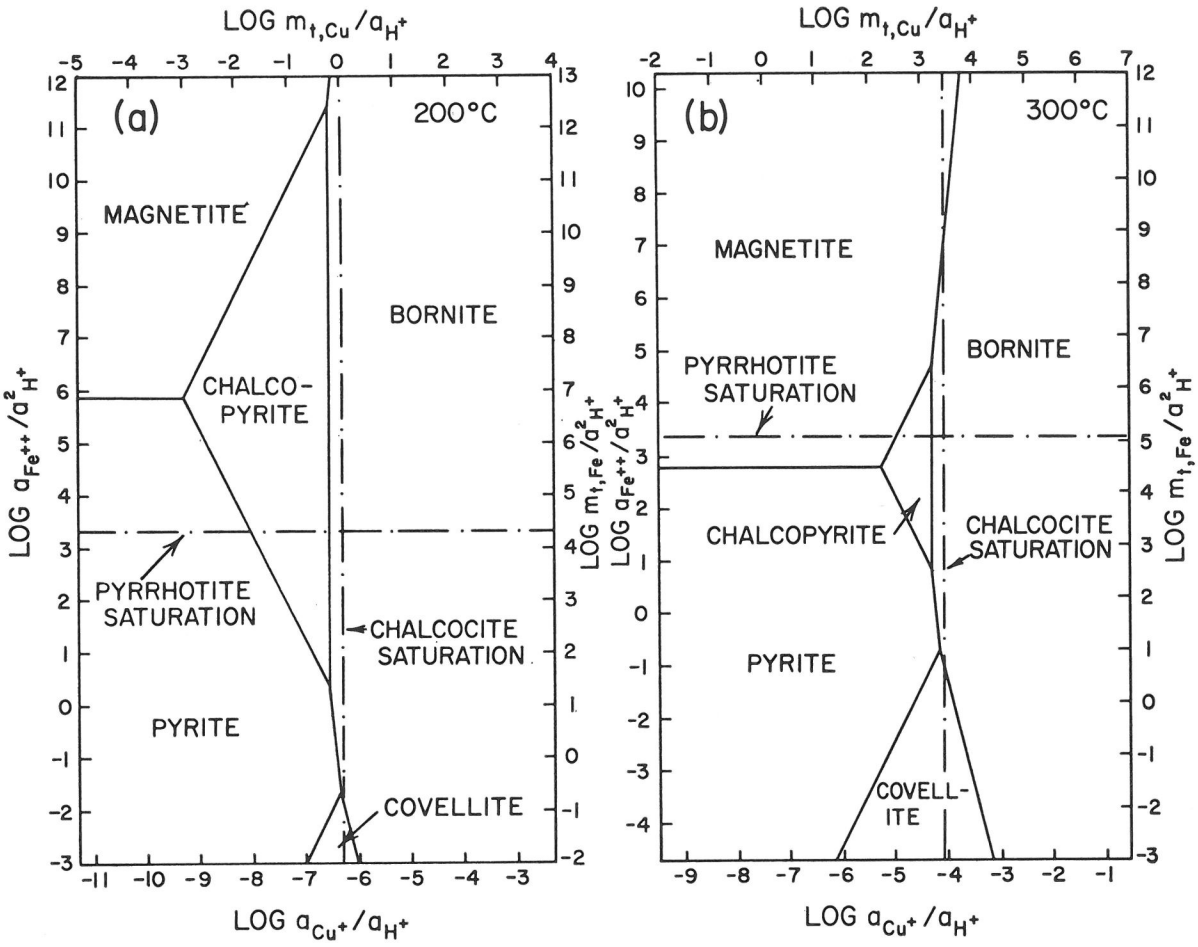

FIG. 9. Abridged theoretical activity diagram for the system $FeCl_2$-CuCl-HCl-H_2S-H_2SO_4-H_2O at one atmosphere, unit activity of H_2O, and 200°C (a) and 300° C (b) for an activity of H_2S in solution of $10^{-2.5}$. The scales on the right side and top of each diagram represent computed solubilities of the minerals in a 3 molal sodium chloride solution (Helgeson, 1969, 1970a).

$$\bar{x}_\phi = \bar{x}_\phi{}^0 + \bar{n}_\phi \Delta\xi + \frac{\bar{n}_\phi{}'(\Delta\xi)^2}{2!} + \cdots \tag{10}$$

where the superscript (°) indicates an earlier stage of reaction progress, and

$$\bar{n}_j{}' = \frac{d\bar{n}_j}{d\xi} = \frac{d^2 m_j}{d\xi^2} \tag{11}$$

$$\bar{n}_\phi{}' = \frac{d\bar{n}_\phi}{d\xi} = \frac{d^2 \bar{x}_\phi}{d\xi^2} \tag{12}$$

Hypothetical equilibrium constants can be computed from the new concentrations of species in solution and compared with those predicted from thermodynamic data to see if the solution has become saturated with a new phase. Repetition of this procedure defines the mass transfer and distribution of species as a function of ξ until overall equilibrium is achieved.

The calculations reported below were carried out on a CDC 6400 computer using a machine program in which provision is included for all of the variables discussed above, except changing activity of H_2O; the detailed theoretical equations and computer program have been presented elsewhere (Helgeson, Brown, Nigrini and Jones, 1970).

Reactions of Hydrothermal Solutions with Granitic Rocks

Predicted changes in solution composition and the sequence and amounts of minerals made and destroyed (kgm $H_2O)^{-1}$ during reaction of acid chloride-rich solutions with rocks of granitic composition at 100°, 200°, and 300°C are shown in Figures 11–33. The initial compositions of the reactant rocks and the aqueous phase are summarized in Table 4; the thermodynamic data used in the calculations are those reported elsewhere (Helgeson, 1969).

The hypothetical rock involved in reactions (1 and 4–7) (Table 4) consists of quartz, microcline, albite, and annite (as a representative of biotite and other ferro-magnesian minerals in the rock). In contrast, an idealized granodiorite

is the reactant rock in reactions 2 and 3, with andesine and high sanidine representing plagioclase and K-feldspar, respectively. In all seven reactions the composition of the rock (in mole fractions of minerals excluding quartz) was taken to be 0.1 K-feldspar, 0.6 plagioclase, and 0.3 annite. These mole fractions were regarded in the calculations as the relative reaction rates for the minerals (Helgeson, 1968; Helgeson, Garrels, and Mackenzie, 1969). The solutions in the eight reactions (Table 4) were selected as "reasonable" hydrothermal fluids using as a guide the general compositional characteristics shown in Table 2. To facilitate the calculations, some of the solutions were considered to be slightly undersaturated at the outset with respect to quartz. In each case the reactions involve acid aqueous solutions at one atmosphere and the indicated temperature.

Reaction with an hypothetical quartz+albite+microcline +annite rock at 200° C. The consequences of reaction 1 (Table 4) are illustrated in Figures 2d and 11–15. The mass of minerals produced and destroyed during reaction progress is shown in Figure 11 as a function of the progress variable, and in Figure 12 as a function of solution pH. Corresponding changes in solution composition and the distribution of aqueous species during reaction progress are illustrated in Table 5 and Figures 13 and 14, respectively. The reaction path is represented in Figure 2d, and the relative percentages of the minerals produced by the reaction are depicted in Figure 15.

1. Sequence of Reaction Products. Reaction of the hypothetical quartz+microcline+albite+annite rock with the acid chloride-rich aqueous phase described in Table 4 (reaction 1) leads first to precipitation of quartz at A in Figures 11–14, and next to the appearance of montmorillonite at B (Figs. 2d and 11–14). It can be seen in Figures 13 and 14 that the molality of ferrous iron and the pH of the solution increase with continued precipitation of montmorillonite and quartz (at the expense of albite, microcline, and biotite) which causes the solution to become saturated with pyrite at A′. Continued reaction results in precipitation of nontmorillonite, quartz, and pyrites in the mass ratio of ~50:25:1 as the molality of Fe^{2+} continues to increase in solution in response to the destruction of biotite. At B′ the solution becomes saturated with chalcopyrite, which then precipitates at the expense of pyrite until all of the pyrite is replaced by chalcopyrite at C′. Continued reaction of the solution with the rock results in precipitation of chalcopyrite, quartz, and montmorillonite along C′C until the solution equilibrates with biotite at C. Further reaction then results in precipitation of secondary biotite along with quartz, montmorillonite, and chalcopyrite until at D′ the solution becomes saturated with bornite. Note that in the interval CD′ the molality of ferrous iron and the activity of the hydrogen ion both decrease substantially, but that of S^{2-} continues to increase until bornite appears at D′ (Figs. 13 and 14). Further reaction causes bornite to replace completely the chalcopyrite precipitated along B′D′ until all of the chalcopyrite is consumed at E′. As bornite continues to precipitate, the solution changes composition to D where it reaches equilibrium with microcline in the reactant rock. Further reaction (of the solution with albite in the rock) causes co-precipitation of microcline, biotite, quartz, montmorillonite and bornite along DF′, until at F′ the solution becomes saturated with chalcocite. Chalcocite then replaces bornite along F′G′ until all of the bornite is consumed at G′. Continued reaction from G′ results in precipitation of microcline, biotite, quartz, montmorillonite, and chalcocite until the solution equilibrates with albite at E, where overall equilibrium is established among the aqueous solution and the minerals in the rock.

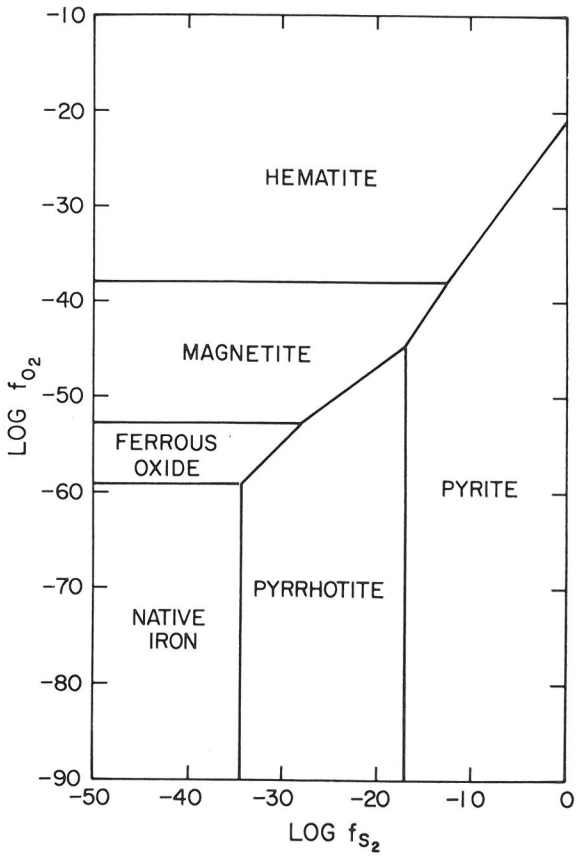

FIG. 10. Theoretical fugacity diagram for the system Fe-S-O at 200°C and one atmosphere (Helgeson, Brown, and Leeper, 1969—reproduced with permission from Freeman, Cooper and Co.).

2. Compositional Changes in the Aqueous Phase. The sequence of events illustrated in Figures 11–15, and in fact in all subsequent figures, occurs in response to the increase in solution pH caused by reaction of the hydrothermal solution with its host rock. It can be seen in Figure 13 that the total concentrations of aluminum and iron in the aqueous phase first increase with reaction progress to B and B′ (which correspond to the appearance of montmoril-

TABLE 4. SUMMARY OF INITIAL COMPOSITIONS OF HYDROTHERMAL SOLUTIONS AND ROCKS CONSIDERED IN THEORETICAL MASS TRANSFER CALCULATIONS

Reaction Number	Temperature (°C)	Initial Solution pH	Initial Solution Composition (log total molality)												
			Al^{3+}	K^+	Na^+	Ca^{2+}	Mg^{2+}	Fe^{2+}	Pb^{2+}	Zn^{2+}	Cu^+	H_4SiO_4	S^{2-}	SO_4^{2-}	CO_2	Cl^-
1	200	3.0	−4.00	−0.301	0.477	—	—	−3.47	—	−2.00	−1.56	−2.36	−4.24	−4.73	—	0.550
2	200	3.0	−4.50	−0.602	0.301	−0.699	—	−7.00	—	—	−3.00	−2.35	−2.30	−2.30	−1.301	0.422
3	200	3.0	−4.00	−0.602	0.301	−0.398	—	−3.20	—	—	−3.22	−2.35	−4.12	−4.30	−1.40	0.484
4	100	3.5	−4.30	−0.301	0.477	—	—	−4.50	—	−2.85	−4.50	−3.15	−6.52	−3.00	—	0.544
5	300	3.0	−4.00	−0.301	0.477	—	—	−2.80	—	−2.00	−2.80	−2.00	−2.90	−3.90	—	0.548
6	300	3.0	−4.00	−0.301	−0.301	—	—	−2.80	—	−2.00	−2.80	−2.00	−2.90	−3.90	—	0.013
7	300	3.0	−4.00	−2.00	−1.301	—	—	−3.00	—	−2.00	−2.80	−2.00	−2.90	−3.90	—	−1.067
8	150	3.0	—	—	−0.523	−7.00	−2.00	−5.00	−5.00	−4.301	−5.00	—	−4.60	−5.50	−7.00	−0.493
9	150	3.0	—	—	−0.523	−7.00	−2.00	−5.00	−5.00	−4.301	−5.00	—	−4.60	−3.80	−7.00	−0.493
10	150	3.0	—	—	0.301	−7.00	−2.00	−4.699	−4.00	−3.301	−3.959	—	−4.00	−4.00	−7.00	0.306
11	150	3.0	—	—	−0.523	−7.00	−2.00	−5.00	−5.00	−4.301	−5.00	—	−4.60	−5.50	−7.00	−0.493
12	150	3.0	—	—	0.301	−7.00	−2.00	−4.699	−4.00	−3.301	−3.959	—	−4.00	−4.00	−7.00	0.306

Reaction coefficients of reactant minerals

Reaction Number	calcite[a]	andesine[b]	microcline[c]	high sandine[d]	biotite (annite)[e]	low albite[f]
1	—	—	0.1	—	0.3	0.6
2	—	0.6	—	0.1	0.3	—
3	—	0.6	—	0.1	0.3	—
4	—	—	0.1	—	0.3	0.6
5	—	—	0.1	—	0.3	0.6
6	—	—	0.1	—	0.3	0.6
7	—	—	0.1	—	0.3	0.6
8	1.0	—	—	—	—	—
9	1.0	—	—	—	—	—
10	1.0	—	—	—	—	—
11	1.0	—	—	—	—	—
12	1.0	—	—	—	—	—

[a] $CaCO_3$ [b] $Ab_{67}An_{33}$ [c] $KAlSi_3O_8$ [d] $KAlSi_3O_8$ [e] $KFe_3AlSi_3O_{10}(OH)_2$ [f] $NaAlSi_3O_8$

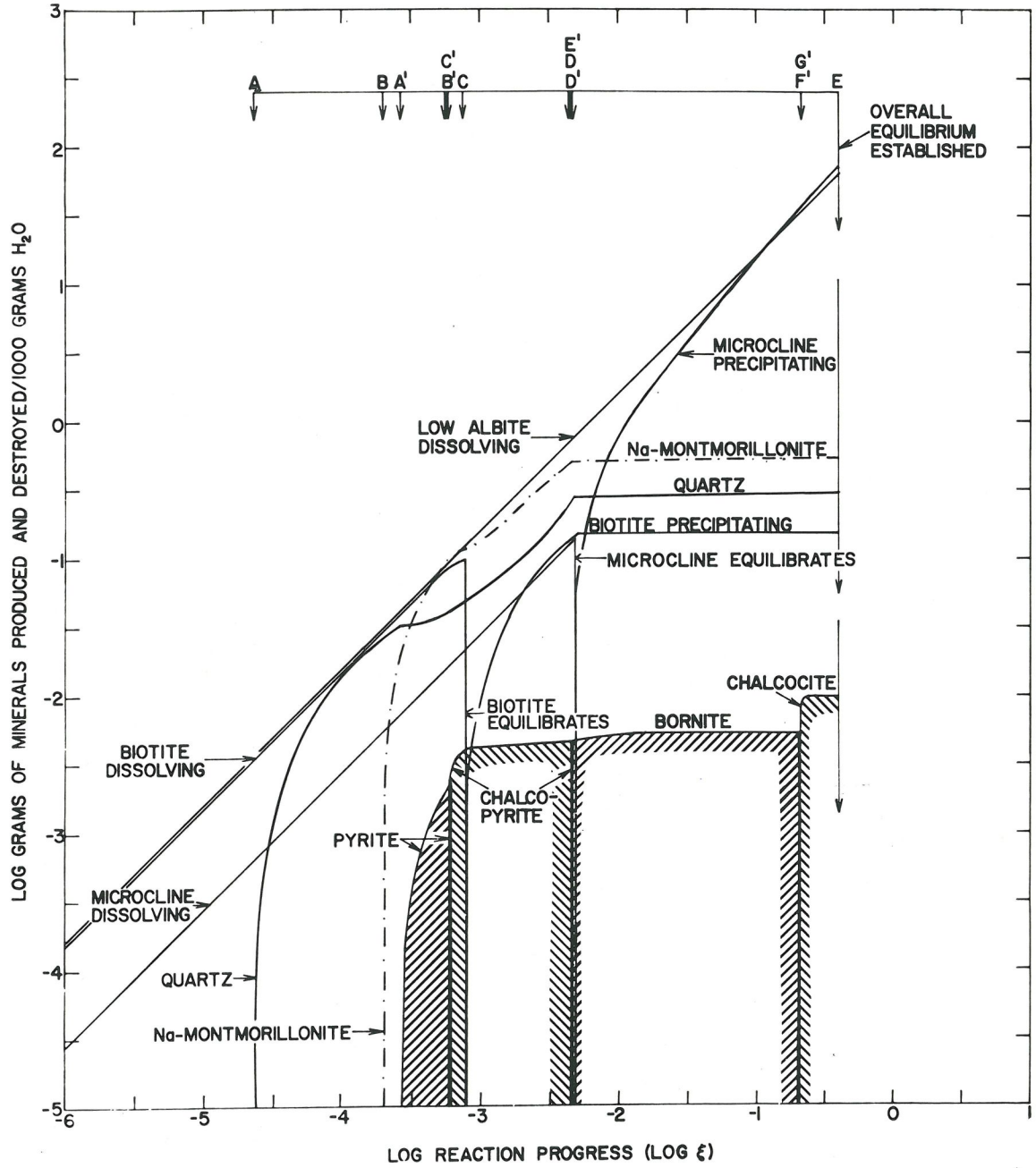

FIG. 11. Mass of minerals produced and destroyed (kgm $H_2O)^{-1}$ as a function of progress in the reaction of an acid chloride-rich hydrothermal solution with an hypothetical quartz+microline+albite+annite rock at 200°C and one atmosphere (reaction 1, Table 4). The arrows and letter annotations at the top of the diagram refer to sequential events in reaction progress (see Figures 2d and 12–14).

lonite and chalcopyrite, respectively), and then decrease as the solution continues to react with its mineralogic environment. Over the entire reaction path the activity of the hydrogen ion decreases by about two orders of magnitude (Figure 13), which causes substantial dissociation of H_2S and a corresponding increase in the molality of the sulfide ion by several orders of magnitude (Figure 14). This change is responsible for the sequential appearance of sulfides with reaction progress. The order in which they appear is a function of the relative magnitude of the total concentrations of the metal ions in solution, the sizes of the solubility product constants of the sulfides, and the relative degrees to which the metal ions are complexed in the aqueous phase.

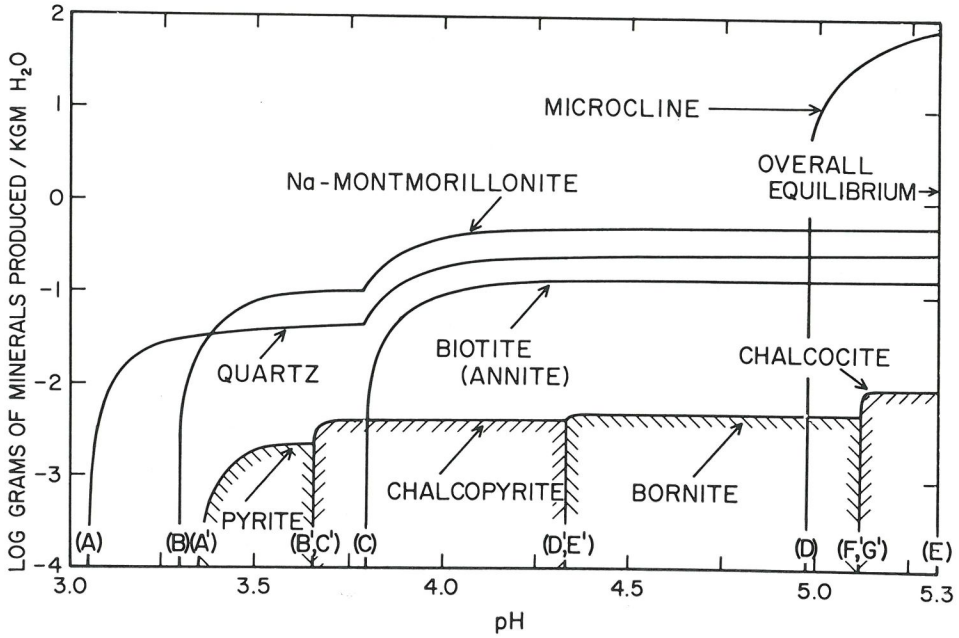

FIG. 12. Mass of minerals produced and destroyed (kgm $H_2O)^{-1}$ as a function of solution pH in the reaction depicted in Figures 2d, 11, and 13–14 (reaction 1, Table 4). The letter annotations refer to sequential events in reaction progress.

It can be deduced from the curves in Figure 14 that the oxidation state of the system (f_{O_2}) steadily decreases with reaction progress. Note that precipitation of biotite +chalcopyrite along CD′ causes the solution composition and distribution of aqueous species to change abruptly (Figs. 13 and 14). In fact, with the appearance of bornite and microcline and the disappearance of chalcopyrite at D′, D, and E′, respectively, the total concentration of aluminum in solution increases nearly a log unit while the activity of H^+ and the total concentrations of S^{2-} and Fe^{2+} decrease about a log unit each over an infinitesimal range of ξ. Note that in this interval the total molalities of Fe^{3+} and Cu^{2+} decrease several log units. In contrast, subsequent reaction progress takes place with only slight changes in the composition of the solution.

The overall mass transfer to and from the aqueous phase in Figures 13 and 14 results in the changes in solution composition summarized in Table 5. It can be deduced from Table 5 that the relatively small concentration of total sulfide in solution limited severely the fraction of total copper abstracted by the precipitation of sulfides, and that the relatively high concentration of Fe^{2+} caused the early appearance of the more iron-rich sulfides. Nevertheless, the grade of copper ore represented by the sulfides in Figures 11 and 12 is about two percent of the mass of quartz precipitated during reaction progress.

3. Relative Mass Transfer. The relative mass of the minerals produced during reaction progress are illustrated in Figure 15. It can be seen that the montmorillonite fraction is high in the early (more acid) stages of reaction progress, but K-feldspar accounts for nearly all of the mass of minerals produced near the end. It can be deduced from Figure 11 that the total redistribution of mass accompanying equilibration of the aqueous phase with its environment is greater than 70 grams (kgm $H_2O)^{-1}$. The reaction results in destruction of 67 grams of albite, 0.1 grams of biotite, and 0.1 grams of K-feldspar, but precipitation of 0.15 grams of biotite, 70.6 grams of K-feldspar, 0.3 grams of quartz, 0.5 grams of montmorillonite, and from 0.002 to 0.009 grams of sulfides (kgm $H_2O)^{-1}$. The net mass of secondary biotite and K-feldspar produced is thus 0.05 and 70.5 grams (kgm $H_2O)^{-1}$, respectively.

The mass transfer computed above is considerably higher than that predicted previously for reaction of an arkose with sea water at elevated temperatures (Helgeson, 1967a). The reason for the difference is the role played by plagioclase feldspar in driving the reaction to overall equilibrium. Where multiple reactants are involved, the late stages of reaction progress are characterized by destruction of large amounts of the last reactant to equilibrate; *i.e.*, the mineral farthest from equilibrium at the outset becomes the sole reactant in the late stages of reaction progress. Because so many solid reaction products are precipitated simultaneously near the end of the reaction process, large amounts of the last reactant mineral must be destroyed in order for the solution to reach equilibrium. The initial composition of the solution, the relative reaction rates (and relative abundances) of the minerals in the reactant rock, and the thermodynamic properties of the phases in the system determine the identity of the last mineral to equilibrate with the aqueous phase.

The sequence of events illustrated in Figures 11–15 can be interpreted in terms of the zonal, paragenetic, and replacement features commonly observed in hydrothermal ore deposits. For example, the predicted order of appearance of the secondary silicates (montmorillonite, biotite, and K-feldspar) is typical of the alteration mineral zoning observed in ore deposits, as is the computed sequence of sulfide mineralization; *i.e.*, the sequential replacement of early pyrite by chalcopyrite, chalcopyrite by bornite, and bornite by chalcocite. Although one or another of these minerals may be missing in a given instance, this paragenetic and zonal pattern corresponds to that observed from the outside toward the center of mineralization at Butte, Montana, Bingham, Utah, and in many other districts. Provision for other minerals that occur in ore deposits, such as enargite and tennantite, could not be included in the calculations owing to the paucity of thermodynamic data for these phases.

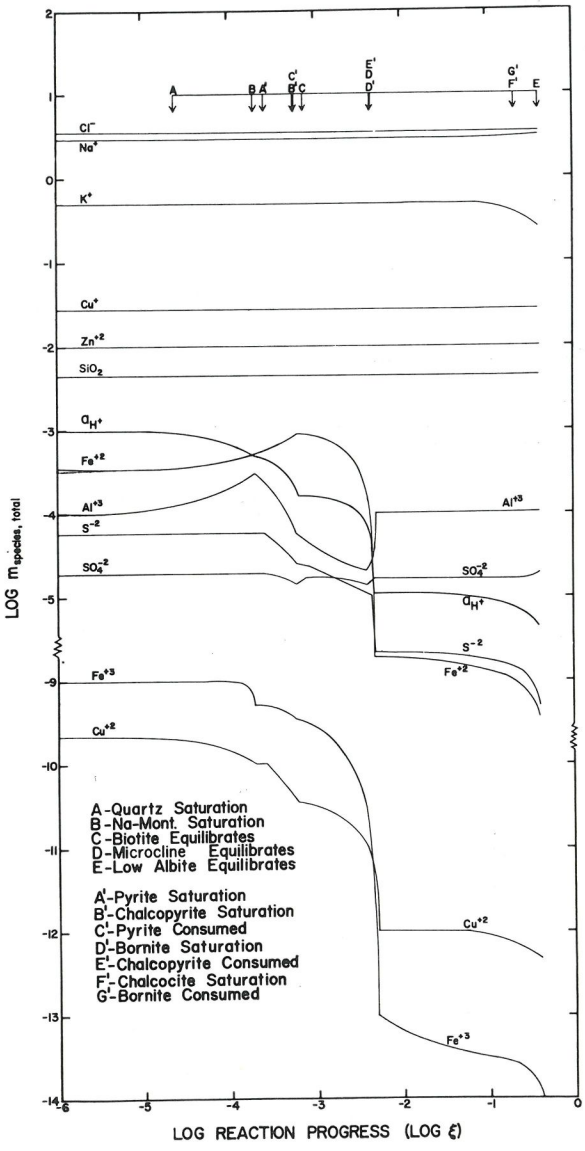

FIG. 13. Total molalities of species (e.g., $m_{H_2S}+m_{HS^-}+m_{S^{2-}}$ = total molality of S^{2-}) in an aqueous phase reacting with an hypothetical quartz+microcline+albite+annite rock at 200°C and one atmosphere (reaction 1, Table 4). The arrows and letter annotations at the top of the diagram refer to sequential events in reaction progress (see Figures 2d, 11, 12, and 14).

TABLE 5. COMPUTED OVERALL CHANGES IN SOLUTION COMPOSITION RESULTING FROM REACTION 1, TABLE 4

Species	Starting Concentration (total ppm)	Final Concentration (total ppm)	Net Change
Al^{3+}	2.2	3.7	1.5
K^+	16,062	7,948	−8,114
Na^+	56,661	61,708	5,047
Fe^{2+}	15.6	0.02	−15.6
Cu^+	1,438	1,437	−1
Fe^{3+}	3.5×10^{-5}	4.0×10^{-10}	-3.5×10^{-5}
Cu^{2+}	1.1×10^{-5}	2.4×10^{-8}	-1.1×10^{-5}
S^{2-}	1.5	0.01	−1.5
SO_4^{2-}	1.5	1.5	0

Reactions with an idealized granodiorite at 200°C. Hypothetical reactions of hydrothermal solutions with a granodiorite consisting of (in mole fractions of minerals excluding quartz) 0.1 sanidine, 0.6 andesine ($Ab_{67}An_{33}$), and 0.3 annite (as a representative of biotite, amphibole and pyroxene) at 200°C are depicted in Figures 16–22. The initial compositions of the aqueous solutions are summarized in Table 4 (reactions 2 and 3). In contrast to the reaction described above, $CaCl_2$ and CO_2 are components in the aqueous phase involved in these reactions.

1. Reaction involving a sulfide (and sulfate)-rich solution. Reaction of the granodiorite with a concentrated sodium-calcium-potassium chloride solution containing (initially) 423 ppm sulfate, 141 ppm sulfide, 56 ppm copper and 0.005 ppm iron (reaction 2, Table 4) is depicted in Figures 16–20. In contrast to the preceding case, the following calculations include provision for the possible appearance of solid solution minerals as reaction products.

It can be seen in Figures 16 and 17 that reaction 2 in Table 4 leads first to the precipitation of quartz and pyrite (in the mass ratio of 1.6:1) at the expense of the minerals in the host rock; i.e., sanidine, andesine, and biotite. As the reaction continues, the solution becomes saturated with montmorillonite at A. Despite the fact that the concentration of sodium is much higher than that of calcium in the aqueous phase, the montmorillonite produced by the reaction has the composition, Ca-beidellite$_{67}$Na-beidellite$_{33}$ ($Ca_{0.115}Na_{0.10}Al_{2.35}Si_{3.67}O_{10}(OH)_2$). A montmorillonite of this composition is precipitated in preference to a more sodic montmorillonite because of the disparity in charge and the size of the activity coefficients of Na^+ and Ca^{2+} in the aqueous phase. Because the absolute concentrations of Ca^{2+} and Na^+ in the hydrothermal solu-

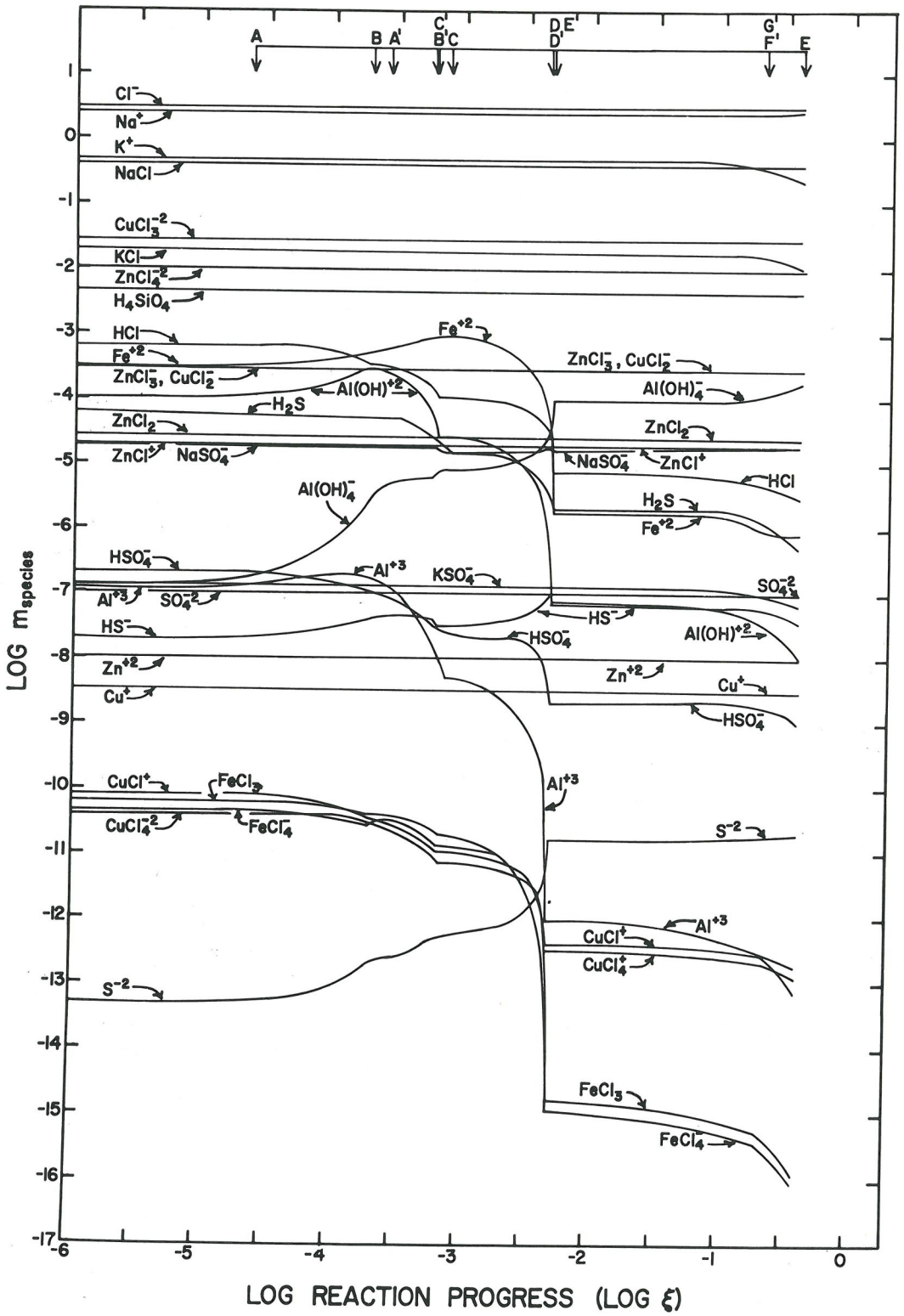

FIG. 14. Molalities of species in the aqueous phase reacting with an hypothetical quartz+microcline+albite+annite rock at 200°C and one atmosphere (reaction 1, Table 4). The arrows and letter annotations at the top of the diagram refer to sequential events in reaction progress (see Figures 2d and 11–13).

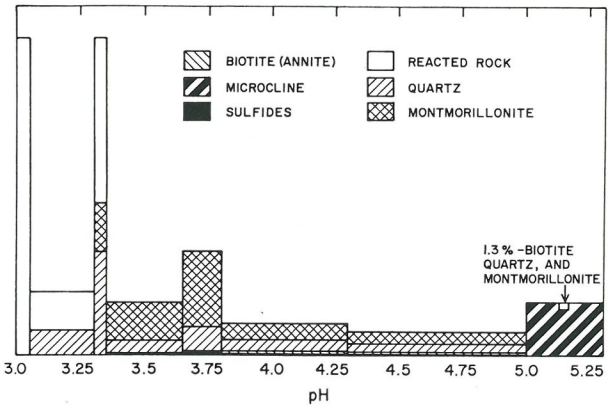

FIG. 15. Relative mass of minerals produced and destroyed (kgm H_2O)$^{-1}$ by the reaction depicted in Figures 2d and 11–14 (reaction 1, Table 4) plotted as a function of solution pH. The fraction of the area corresponding to a mineral in each circumscribed interval (all of which have equal areas) is equal to the relative mass of the mineral. For example, the mass of minerals produced in the interval of reaction progress over which the solution pH changes from 3.35 to 3.65 consists of ~70% montmorillonite, ~28% quartz, and ~2% sulfide (pyrite). The total area outlined for this interval equals that in all others.

tion are large relative to the mass transfer of these ions to or from the aqueous phase, the ratio of their concentrations remains essentially constant throughout the reaction process illustrated in Figures 16–20, which causes the composition of the montmorillonite reaction product to remain constant.

Continued reaction beyond A in Figures 16, 17, and 18 causes precipitation of montmorillonite, pyrite, and quartz in mass ratios varying from 1:1:1 to ~4:2:1. At B (Figs. 16–20) the solution becomes saturated with bornite, and along BC bornite co-precipitates with pyrite, quartz, and montmorillonite. The mass ratio of pyrite to bornite reaches 6.3 along this segment of the reaction path. At C, calcite joins the assemblage of reaction products, which causes the abrupt disappearance of bornite. Along CD, pyrite replaces bornite until all of the bornite is consumed at D. With further reaction progress the solution becomes saturated with biotite at E, which inhibits further precipitation of pyrite. Continued reaction from E results in precipitation of montmorillonite, quartz, calcite, biotite, and minor pyrite until the solution becomes saturated with chalcopyrite at F. Chalcopyrite and biotite then replace pyrite along FG. The solution becomes saturated with K-feldspar at G, which causes andesine and quartz to be replaced by K-feldspar until the solution becomes saturated with laboradorite ($Ab_{43}An_{57}$) at H. Continued reaction from H produces calcite, K-feldspar, biotite, chalcopyrite, and laboradorite at the expense of andesine, quartz, and pyrite until the activity ratio of Na^+ to Ca^{2+} in the aqueous phase changes appreciably toward an equilibrium value for the andesine in the host rock. When this occurs, the secondary laboradorite changes composition and approaches that of andesine, and the montmorillonite reacts with the solution to become more sodic until overall equilibrium is achieved. This last stage of reaction progress is not illustrated in Figures 16–20.

The sequence of events and relative mass of minerals

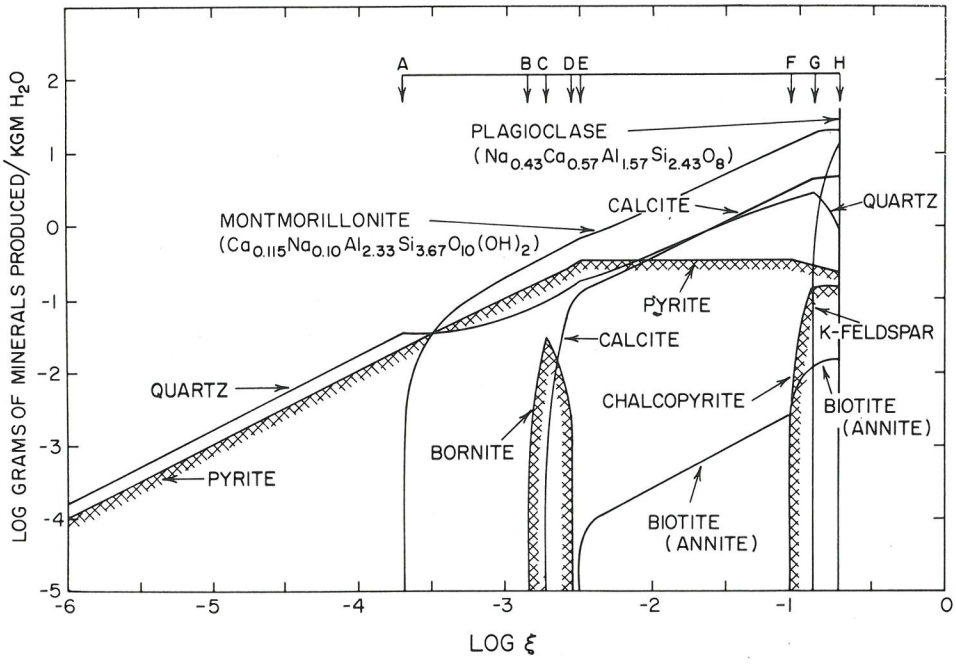

FIG. 16. Mass of minerals produced (kgm H_2O)$^{-1}$ as a function of progress in the reaction of an acid chloride-rich hydrothermal solution with an hypothetical granodiorite at 200°C and one atmosphere (reaction 2, Table 4). The arrows and letter annotations at the top of the diagram refer to sequential events in reaction progress (see Figs. 17–20).

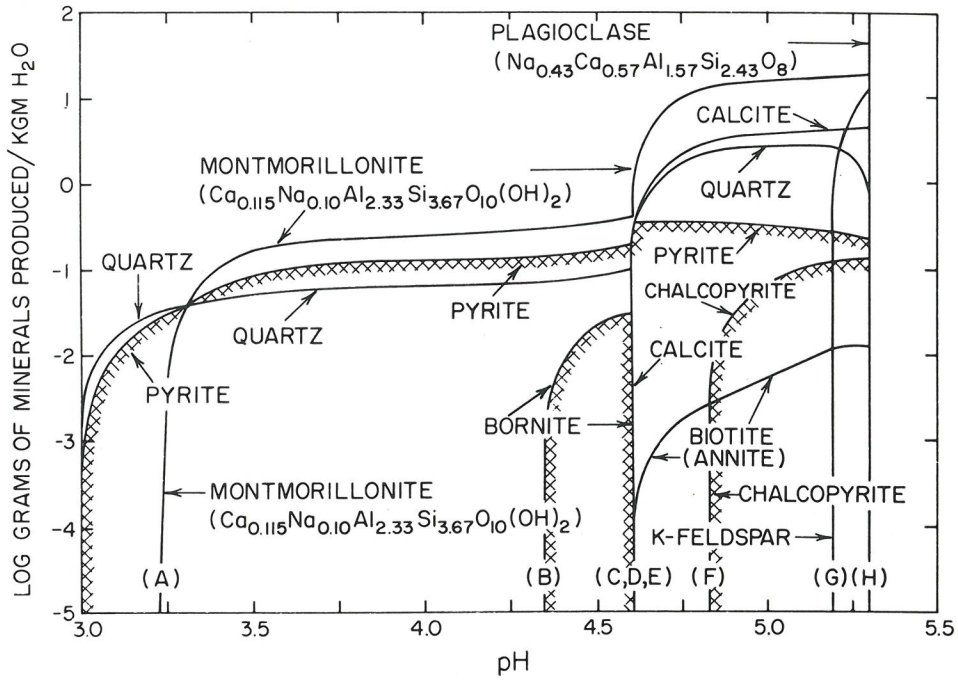

FIG. 17. Mass of minerals produced (kgm H_2O)$^{-1}$ as a function of solution pH in the reaction depicted in Figures 16 and 18–20 (reaction 2, Table 4). The arrows and letter annotations at the top of the diagram refer to sequential events in reaction progress.

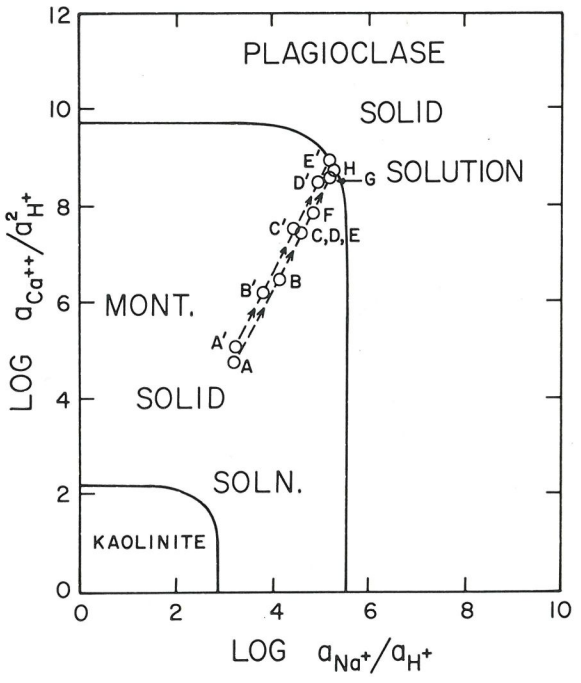

FIG. 18. Theoretical activity diagram for the system NaCl-HCl-$CaCl_2$-Al_2O_3-SiO_2-H_2O in the presence of quartz and an aqueous phase at 200°C, one atmosphere, and unit activity of H_2O. The stability fields were drawn assuming ideal solid solution using thermodynamic data taken from Helgeson (1969). The dashed lines, arrows, and letter annotations refer to the reactions depicted in Figures 16–17, and 19–21 (reactions 2 and 3, Table 4).

produced as a result of the overall reaction described above are illustrated in the paragenesis diagram depicted in Figure 20. It can be seen in this figure that in the late stages of reaction progress, quartz, K-feldspar, and calcite are produced in roughly equivalent amounts, and that the amount of chalcopyrite precipitated is equal to approximately one percent of the mass of these reaction products; copper is present to the extent of one percent of the mass of calcite and quartz produced by the reaction. Approximately 30 grams of granodiorite (kgm H_2O)$^{-1}$ are destroyed along reaction path AH.

During the reaction illustrated in Figures 16–20, 2 ppm aluminum and 1,448 ppm sodium are added to the aqueous phase, and 1,064 ppm potassium, 550 ppm calcium, 41 ppm copper, 137 ppm sulfide, and 48 ppm sulfate are removed. In the process, approximately 0.5 grams of biotite are pyritized, 0.14 grams of chalcopyrite are precipitated (at the expense of pyrite), and the mass ratio of pyrite to chalcopyrite decreases to 1.7. The fugacity of O_2 decreases by 0.8 log units over the reaction path and the fugacity of CO_2 drops from 10 to 0.5 atmospheres. In contrast, the fugacity of S_2 decreases 5.6 log units. The sulfate ion serves as a reservoir for sulfide during the reaction process; *i.e.*, it is reduced by the pyritization of biotite to maintain equilibrium among the sulfides and the aqueous phase.

As indicated above, the appearance of calcite causes drastic changes in the chemistry of the solution and the assemblage of minerals produced in the late stages of reaction progress. It can be deduced from Figure 19 that the

appearance of calcite temporarily buffers the pH of the aqueous phase. This buffering effect continues as long as the concentrations of CO_2 and Ca^{2+} in solution exceed the mole transfer of these species to or from the aqueous phase (Figure 19). Under these conditions equilibrium with calcite requires a constant solution pH, which prevails until the concentration of CO_2 in the aqueous phase decreases significantly as a function of continued reaction progress. Because the solution pH remains constant along GDE, continued reaction of the solution with its host rock to produce pyrite (among other minerals) causes a decrease rather than an increase in the activity of the sulfide ion along this segment of the reaction path; hence bornite and pyrite cannot continue to co-precipitate beyond C. Instead, pyrite replaces bornite, and finally biotite appears as a reaction product at E.

Various chemical and geologic implications of the appearance of "early" calcite, pyritization of the wall rock, and the paragenetic, zonal, cotectic and peritectic relations discussed above can be derived from the diagrams in Figures 16–20. However, such generalizations are better deferred until we have examined the effects of other variables on the mass transfer involved in hydrothermal alteration and sulfide deposition.

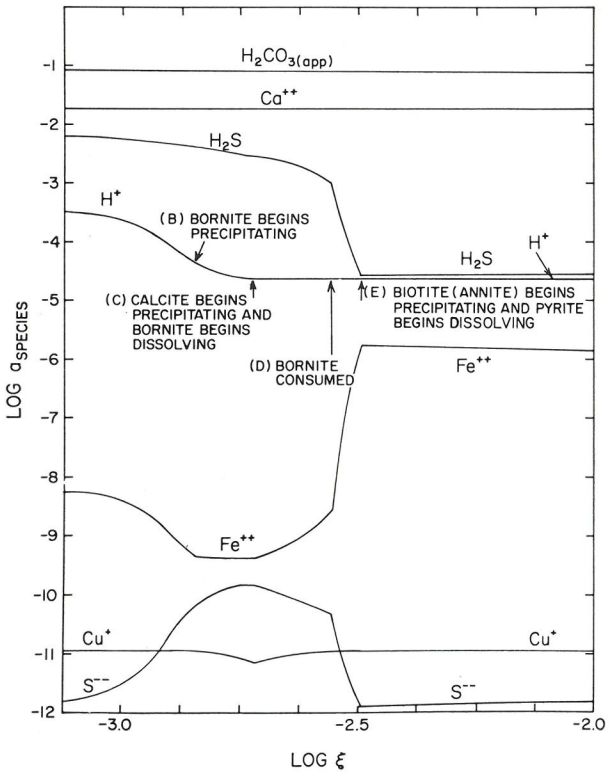

FIG. 19. Activities of species in the aqueous phase reacting with an hypothetical granodiorite at 200°C and one atmosphere (reaction 2, Table 4). The arrows and letter annotations refer to sequential events in reaction progress (see Figs. 16–18 and 20). The subscript (app) indicates that the species represents the sum of H_2CO_3 and CO_2 (aq).

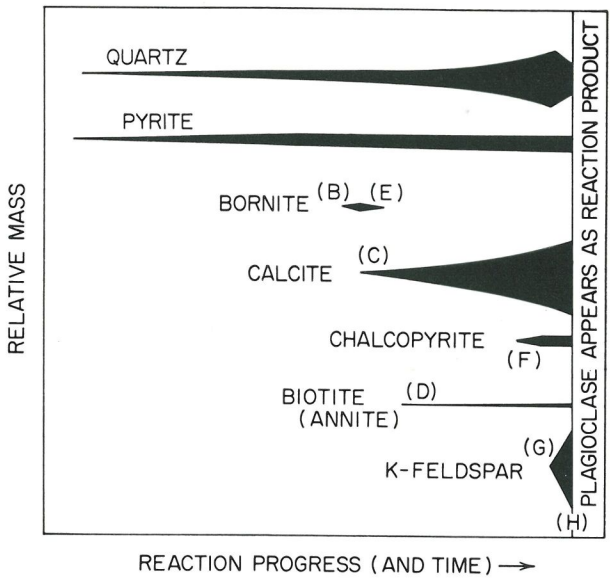

FIG. 20. Paragenesis diagram depicting the relative mass of minerals produced as a function of progress in the reaction depicted in Figures 16–19 (reaction 2, Table 4).

2. Reaction involving sulfide (and sulfate)-deficient solutions. Reaction of a granodiorite with a sulfide-deficient hydrothermal solution (reaction 3, Table 4) is depicted in Figures 18, 21, and 22. By comparing Figures 17 and 21 it can be seen that reactions involving either sulfide-rich or sulfide-deficient solutions lead to the same assemblage of reaction products, except for the occurrence of early bornite in reaction 2 (Figure 17). Because of the lower sulfide and sulfate concentrations in the aqueous phase involved in reaction 3 (Figure 21), the amount of pyrite produced in this reaction is nearly 100 times less than that in reaction 2. Note also in Figure 21 that the appearance of biotite as a reaction product causes leaching of earlier formed pyrite. Because no sulfide other than pyrite is formed in the early stages of reaction 3 (in contrast to reaction 2), the chemistry of the system is little affected by the temporary pH constraint imposed by the appearance of calcite. On the other hand, the total mass of silicate and carbonate minerals produced in the two reactions is comparable. Ore concentrations of bornite and/or chalcopyrite are produced in reaction 2 (Figure 17), but the mass of chalcopyrite precipitated in reaction 3 (Figure 21) is more than two orders of magnitude less than that precipitated in reaction 2. In contrast, the mass ratio of chalcopyrite to pyrite is higher in the latter case.

Because the activity of H_2S in the aqueous phase decreases only slightly along A″A′B′C′D′E′ (Figures 18 and 21), the reaction path can be approximated on the equilibrium activity diagram depicted in Figure 22. It can be deduced from this diagram that the appearance of biotite as a reaction product at B′ has a strong influence on the relative change in the chemical potentials of the components $FeCl_2$ and CuCl with continued reaction progress.

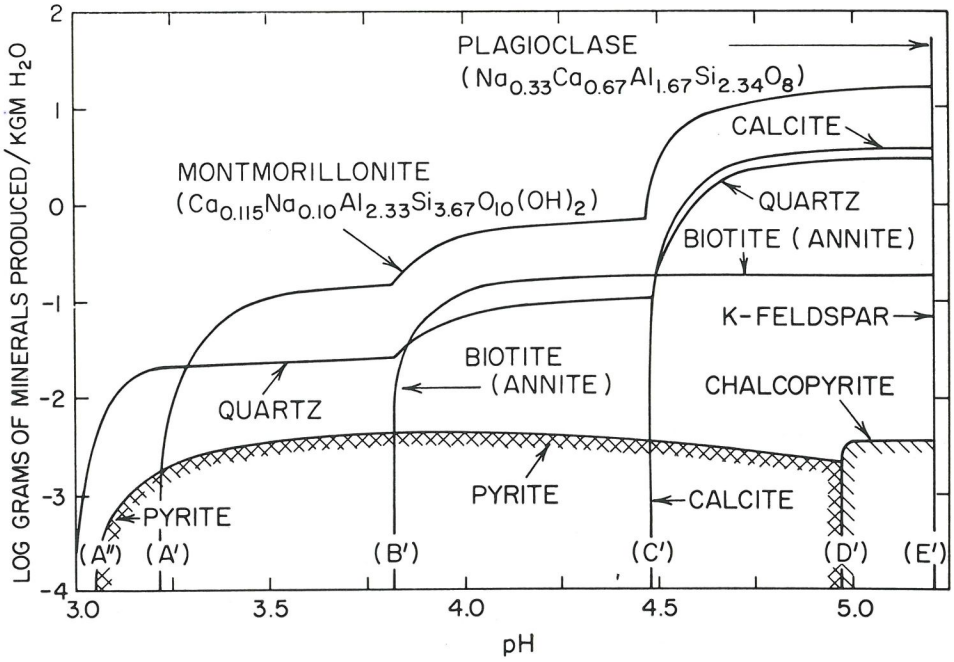

FIG. 21. Mass of minerals produced (kgm $H_2O)^{-1}$ as a function of progress in the reaction of an acid chloride-rich, sulfide (and sulfate)-deficient hydrothermal solution with an hypothetical granodiorite at 200°C and one atmosphere (reaction 3, Table 4). The letter annotations refer to sequential events in reaction progress (see Figs. 18 and 22).

The activity of Fe^{2+} in the aqueous phase increases as biotite dissolves and pyrite precipitates along A''A'B'. Further reaction of the solution with K-feldspar and plagioclase causes precipitation of biotite (in part at the expense of pyrite), which is accompanied by a drastic decrease in the activity of Fe^{2+} in solution. This change causes an abrupt shift in the direction of the reaction path in Figure 22, which determines the identity of later reaction products. It can be seen in Figure 22 that the appearance of biotite at B' is responsible for later saturation with chalcopyrite. If the solution had not reached saturation with biotite, magnetite would have appeared instead of chalcopyrite at a later stage of reaction progress. The presence or absence of secondary biotite (or chlorite) may thus be an important discriminant factor in the formation of copper-rich (as compared with iron-rich) ore deposits.

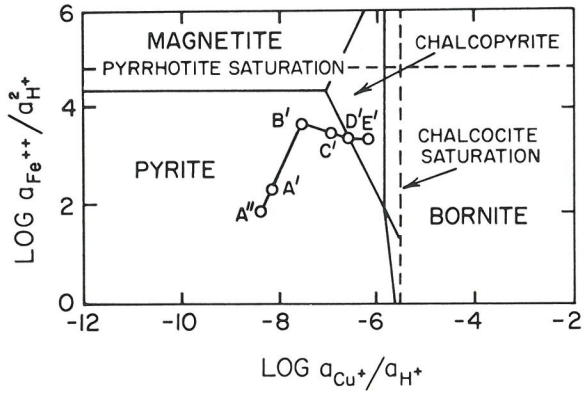

FIG. 22. Theoretical activity diagram for the system $FeCl_2$-CuCl-HCl-H_2S-H_2SO_4-H_2O in the presence of an aqueous phase in which $a_{H_2O}=1.0$ and $a_{H_2S}=10^{-4}$ at 200°C and one atmosphere. The letter annotations and lines connecting the circles refer to the reaction depicted in Figs. 18 and 21 (reaction 3, Table 4).

Reaction with an hypothetical quartz+albite+microcline +annite rock at 100°C. Reaction of the hypothetical quartz+albite+microcline+annite rock discussed above with an acid chloride-rich hydrothermal solution at 100°C (reaction 4, Table 4) is represented in Figures 2a and 23. The reaction involves the same reactant rock and a solution with a similar composition to that in the first reaction discussed above (reaction 1, Table 4). The effect of a 100° difference in temperature on the mass transfer resulting from the reaction can thus be deduced by comparing Figures 11 and 23. Such comparison reveals that the sequence of events at the two temperatures is substantially different.

The reaction at 100°C leads first to the appearance of kaolinite at A in Figure 23, and then to saturation with quartz at B. With continued reaction, pyrite appears as a reaction product at A', but almost immediately afterward the solution becomes saturated with bornite at B', which then replaces the earlier formed pyrite. After destruction of all the pyrite at C', bornite continues to precipitate together with kaolinite and quartz along C'C. At C the solution equilibrates with biotite, which then co-precipitates with kaolinite, quartz, and bornite along CD until the solution becomes saturated with muscovite at D. In

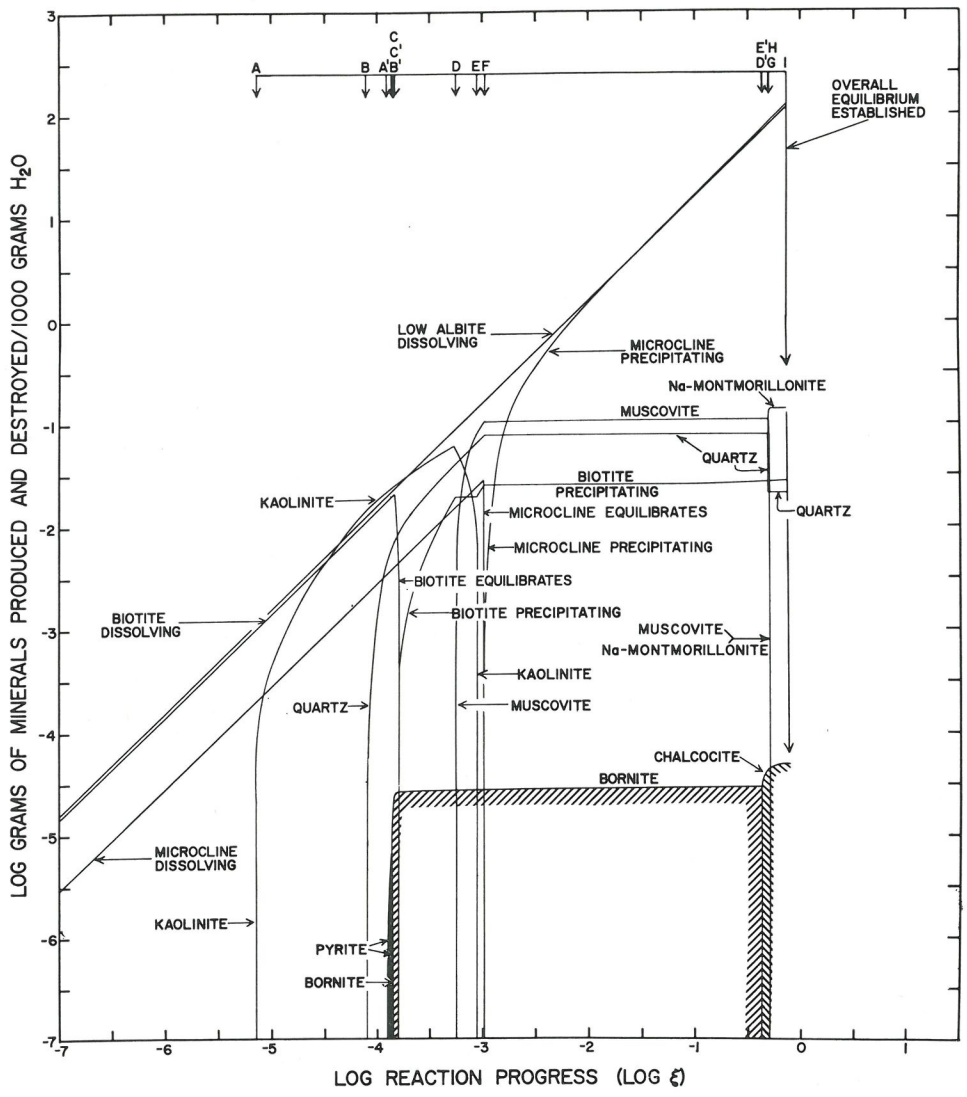

FIG. 23. Mass of minerals produced and destroyed (kgm H_2O)$^{-1}$ as a function of progress in the reaction of an acid chloride-rich hydrothermal solution with an hypothetical quartz+microcline+albite+annite rock at 100°C and one atmosphere (reaction 4, Table 4). The arrows and letter annotations at the top of the diagram refer to sequential events in reaction progress (see Fig. 2a).

the interval DE, muscovite, quartz, and bornite form (in equilibrium with biotite and the aqueous phase) at the expense of kaolinite, K-feldspar and albite until all of the kaolinite is consumed at E. Continued reaction along EF results in deposition of relatively small amounts of biotite, muscovite, quartz, and bornite as the solution approaches saturation with K-feldspar at F. K-feldspar then forms at the expense of albite in the interval FD′ while the solution remains in equilibrium with biotite, muscovite, quartz, and bornite. At D′ the solution reaches saturation with chalcocite, which then replaces bornite until all of the bornite is consumed at E′. Continued reaction causes further precipitation of chalcocite and K-feldspar while the solution maintains equilibrium with biotite, muscovite, and quartz. At G the solution becomes saturated with montmorillonite, which then forms at the expense of muscovite, quartz, and albite. Upon comsumption of all the muscovite at H, further reaction of the solution with albite leads to overall equilibrium among K-feldspar, albite, montmorillonite, quartz, chalcocite, and the aqueous phase at I.

It can be seen in Figure 23 that the total mass of secondary silicate minerals precipitated in the reaction at 100° is only about 0.5 log units lower than that at 200° (Figure 11), but the total mass of sulfides produced is approximately 2 log units lower. Note that chalcopyrite is missing from the sequence of sulfides at 100°, *and that nearly twice as much of the host rock is destroyed at the lower temperatures than at 200°C*. These observations indicate that the lower temperature reaction leads to a sizeable decrease in

volume, which is consistent with precipitation of quartz, sulfides, and other reaction products in open spaces.

The changes in solution composition along reaction path ABCDEFGHI in Figures 2a and 23 include addition of 8,200 ppm sodium to the solution, and removal of 1 ppm aluminum, 13,300 ppm potassium, 2.5 ppm iron, 0.03 ppm copper and 0.008 ppm sulfide. Over the entire reaction path the total concentration of sulfate remains essentially constant, but the fugacity of O_2 drops nearly a log unit and the fugacity of S_2 decreases about 8 log units.

Although various geothermometers indicate higher temperatures than 100°C in the Butte ore deposit, the predicted sequence of events represented by ABCDEFGHI in Figures 2a and 23 corresponds approximately to the distribution of alteration minerals in the wall rocks of the hydrothermal veins at Butte (e.g., see Meyer and Hemley, 1967); *i.e.*, B corresponds to the advanced argillic assemblage immediately adjacent to the veins, D to the kaolinite-sericite boundary farther out in the wall rock, F to the sericite-K-feldspar zone, G to the intermediate argillic assemblage (sans kaolinite) and I to the far interface of the argillic alteration zone with the unaltered rock. In part, the predicted sequence of silicate reaction products also corresponds roughly to the observed zonation of alteration minerals from the outer margins toward the center of porphyry copper deposits; *i.e.*, sericite alteration in the outer zones and secondary K-feldspar and biotite in the inner zones. The predicted sequence of sulfide mineralization along A′B′C′D′E′ in Figure 23 is not an uncommon paragenetic and zonal sequence in hydrothermal systems, and the relative mass of alteration minerals precipitated along path ABCDEFGHI (≃5:4:3:1 for the mass of montmorillonite: muscovite: quartz: biotite) is approximately consistent with that observed in ore

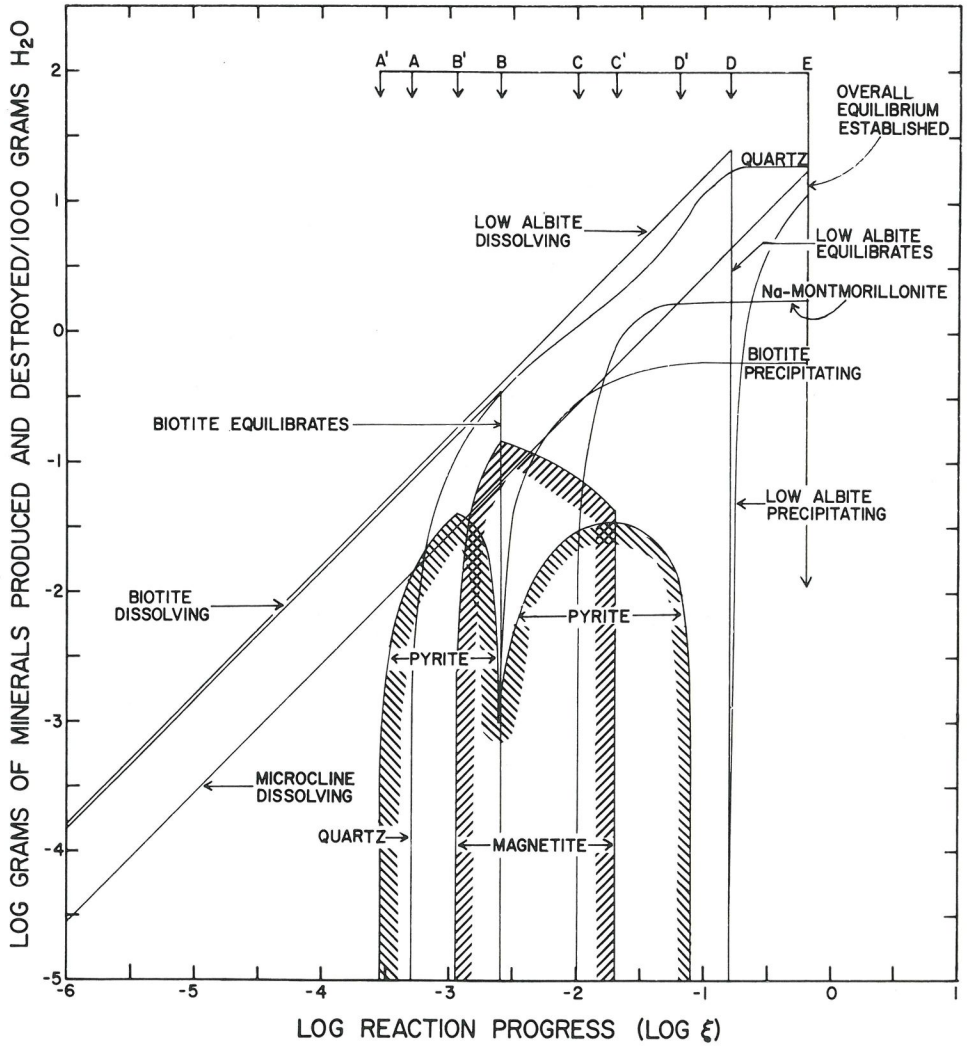

FIG. 24. Mass of minerals produced and destroyed (kgm $H_2O)^{-1}$ as a function of progress in the reaction of an acid chloride-rich hydrothermal solution with an hypothetical quartz+microcline+albite+annite rock at 300°C and one atmosphere (reaction 5, Table 4). The arrows and letter annotations at the top of the diagram refer to sequential events in reaction progress (see Figs. 2c, 25, and 26).

deposits. On the other hand, the common association of sericite and pyrite, and the chalcopyrite mineralization so typical of porphyry copper deposits is not evident in Figure 23. Also, the predicted total mass of rock altered by a liter of solution is considerably greater than that computed from material balance requirements for the mass of hydrogen ion exchanged in the alteration process at Butte (Linn, 1957, unpublished report, Department of Geological Sciences, Harvard University; Meyer and Hemley, 1967; Helgeson, 1964, 1970c; Raymahashay and Holland, 1969). These contradictions no doubt reflect differences in the temperature and solution composition used in the model calculations and that involved in the formation of the Butte ore deposit.

Reactions with an hypothetical quartz+albite+microcline +annite rock at 300°C. Reaction of the hypothetical quartz+K-feldspar+albite+annite rock discussed above with concentrated and dilute acid alkali-chloride solutions in 300°C (reactions 5, 6, and 7, Table 4) are depicted in Figures 2c and 24–31.

1. Reaction involving a concentrated alkali-chloride solution. It can be seen in Figure 24 that reaction of the rock at 300°C with the most concentrated solution (reaction 5, Table 4) fails to lead to the appearance of a copper or copper-iron sulfide, despite the presence in the aqueous phase of 84 ppm copper, 73 ppm iron and 34 ppm sulfide. On the other hand, the reaction produces two generations of pyrite. Pyrite is the first mineral to precipitate from solution (at A′, Figures 24–26) as the rock reacts with the aqueous phase. Quartz joins pyrite as a reaction product at A, and along AB′ the two phases co-precipitate from solution. At B′ the solution becomes saturated with magnetite, and magnetite then begins to replace pyrite. However, before all the pyrite is consumed the solution reaches saturation with biotite at B, which reverses the roles of pyrite and magnetite; *i.e.*, the appearance of biotite causes pyrite to replace magnetite along BC. At C the solution becomes saturated with montmorillonite, which then precipitates together with pyrite, biotite, and quartz at the expense of K-feldspar, albite and magnetite along CC′. After all the magnetite has been replaced by pyrite at C′, biotite continues to precipitate, which causes pyrite to dissolve again until it is all consumed at D′. Biotite thus replaces pyrite along C′D′. Continued reaction results in equilibration of the solution with albite at D, after which quartz, albite, montmorillonite, and biotite co-precipitate in the mass ratio of ∽40:20:3:1 until equilibrium is established with K-feldspar at E.

The solution reaches equilibrium with albite before it equilibrates with K-feldspar in reaction 5 because of the relatively high m_{Na^+} to m_{K^+} ratio in the aqueous phase. Note that during the reaction process more than 0.1 grams of magnetite and 0.03 grams of pyrite (kgm $H_2O)^{-1}$ are produced, and more than 100 grams of rock (kgm $H_2O)^{-1}$ are destroyed. To reiterate briefly for later comparison, the sequence of events involving pyrite and magnetite in the reaction is: (1) precipitation of pyrite, (2) replacement of pyrite by magnetite, (3) replacement of magnetite by pyrite, and (4) dissolution of pyrite.

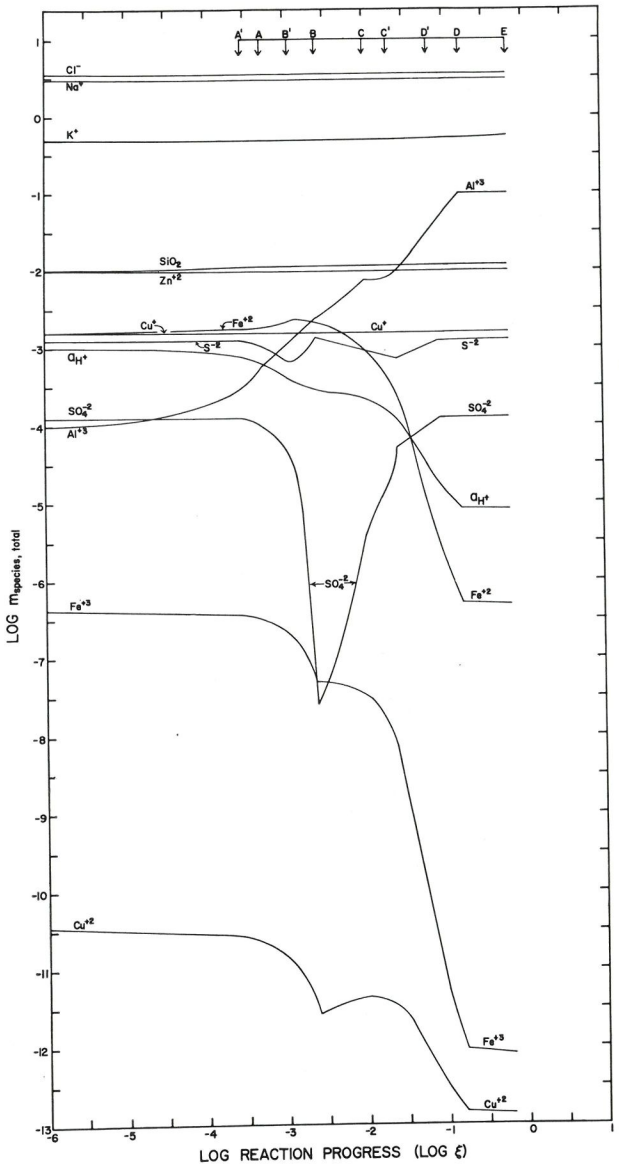

FIG. 25. Total molalities of species in an aqueous phase reacting with an hypothetical quartz+microcline+albite+annite rock at 300°C and one atmosphere (reaction 5, Table 4). The arrows and letter annotations at the top of the diagram refer to sequential events in reaction progress (see Figs. 2c, 24, and 26).

The cause of the double generation of pyrite in Figure 24 can be explained in terms of the changing chemistry of the aqueous phase depicted in Figure 25. It can be seen that precipitation of pyrite (in the early part of the reaction process) along A′B′ is accompanied by a gradual decrease in the total concentration of sulfate in solution. However, the appearance of magnetite at B′, and the subsequent replacement of pyrite by magnetite along B′B

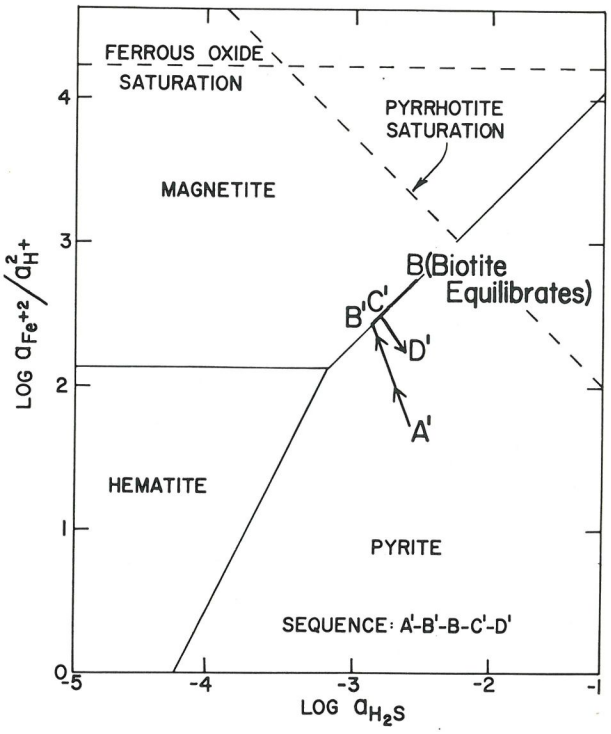

FIG. 26. Theoretical activity diagram for the system $FeCl_2$-HCl-H_2S-H_2SO_4-H_2O in the presence of an aqueous phase at 300°C, one atmosphere, and unit activity of H_2O. The arrows and letter annotations refer to the reaction depicted in Figs. 2c, 24, and 25 (reaction 5, Table 4).

results in a drastic decrease in the total concentration of sulfate. Precipitation of magnetite causes reduction of sulfate to sulfide corresponding to a decrease in the fugacity of O_2 of several orders of magnitude over this segment of the reaction path. Equilibration of the solution with biotite at B stops precipitation of magnetite. With continued reaction, biotite and magnetite exchange their former roles; i.e., magnetite supplies the iron required for precipitation of biotite along BC′, which causes the total concentration of sulfate and the fugacity of O_2 to reverse their previous trend and increase drastically. Pyrite stops dissolving in response to this reversal, which causes precipitation of pyrite until all of the magnetite is consumed at C′. Pyrite then takes over the role played by magnetite in supplying iron for the formation of biotite until it too is consumed at D′. The second generation of pyrite is thus a function of the minimum in the fugacity of O_2 caused by the appearance of biotite as a reaction product. The reversal in the reaction path is illustrated in Figure 26 in terms of log a_{H_2S} and log $a_{Fe^{2+}}/a_{H^{2+}}$ in the aqueous phase.

2. Reaction involving a semiconcentrated alkali-chloride solution. Essentially the same reaction as that described above is depicted in Figures 2c and 27–29, except that the aqueous phase involved in the reaction (reaction 6, Table 4) has a lower concentration of alkali chlorides (34,425 ppm chloride compared with 102,980 ppm in reaction 5). It can be seen by comparing Figures 24 and 27 that the same sequence of reaction products is produced in the two reactions, except for the appearance of sphalerite at the end of reaction 6. On the other hand, reaction of the rock with the less concentrated fluid (Fig. 27) separates out (in terms of ξ) the two generations of pyrite produced in the reaction. The hiatus causes the reaction path to pass up into the magnetite field along C‴B″ in Figures 28 and 29, rather than remaining on the pyrite-magnetite boundary as in the previous reaction (Figure 26). The separation occurs in the more dilute case because the solution fails to equilibrate with biotite before all of the early pyrite is replaced by magnetite. Changes in the fugacities of S_2 and O_2 along the reaction path are illustrated in Figure 29. These changes are similar to those discussed above for the reaction involving the more concentrated solution. Note in Figure 29 that the overall reaction path is considerably more complex than that computed by Raymahashay and Holland (1969) for the reaction of an hydrothermal solution with magnetite.

3. Reaction involving a dilute alkali-chloride solution. Evaluation of the effects of lowering even further the concentration of alkali-chloride in the aqueous phase on the reaction paths discussed above can be made in Figures 30 and 31, which depict reaction on the hypothetical quartz +microcline+albite+annite rock with a dilute hydrothermal solution (reaction 7, Table 4) containing a low concentration of alkali-chloride (3,020 ppm chloride). Comparison of Figures 24, 27, and 30 reveals that the very dilute solution (Fig. 30) produces the same sequence of events in the early stages of reaction progress as that resulting from reaction with the more concentrated solutions: *i.e.*, early precipitation of pyrite with subsequent replacement of pyrite by magnetite, and precipitation of quartz. However, later events in the very dilute case are quite different from those in the reactions involving more concentrated solutions.

Because the ore-forming metal ions (except Fe^{2+}) associate to a considerable degree with the chloride ion to form aqueous complexes in hydrothermal solutions (Helgeson, 1964, 1969), a decrease in the concentration of the chloride ion is accompanied by an increase in the activities of the "free" metal ions in solution. For this reason, the very dilute aqueous phase in reaction 7 becomes saturated with chalcopyrite shortly after reaching quartz saturation (Figures 30 and 31). In contrast, the other two reactions failed to produce a copper-iron sulfide. It can be seen in Figures 30 and 31 that continued reaction results in replacement of pyrite by both chalcopyrite and magnetite. After all the pyrite is consumed, chalcopyrite and magnetite continue to co-precipitate with quartz until the decreasing fugacity of O_2 accompanying precipitation of magnetite causes chalcopyrite to start dissolving. Magnetite then replaces chalcopyrite until biotite appears as a reaction product. As in the case of the double generation of pyrite discussed above, the appearance of biotite reverses the change in the fugacity of O_2 with further reaction pro-

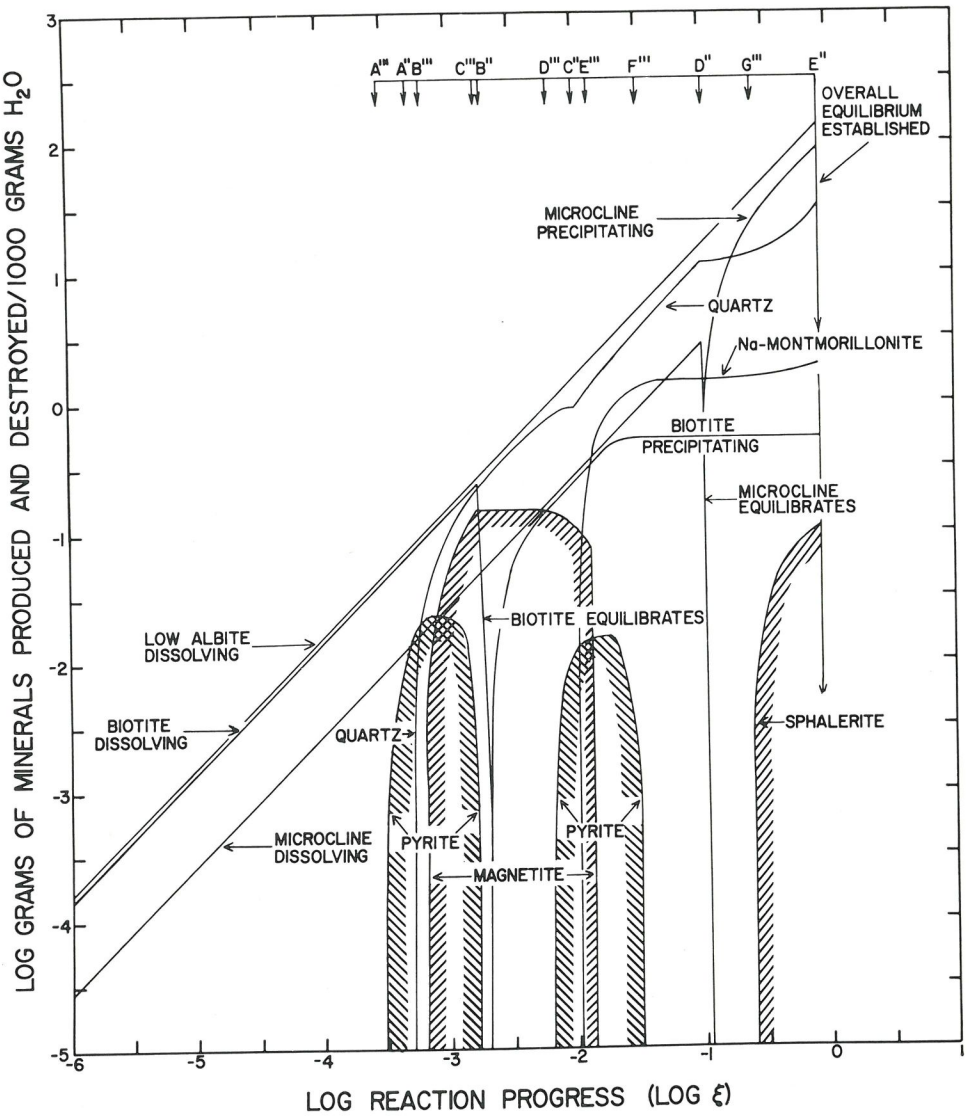

FIG. 27. Mass of minerals produced and destroyed (kgm H_2O)$^{-1}$ as a function of progress in the reaction of an acid hydrothermal solution with an hypothetical quartz+microcline+albite+annite rock at 300°C and one atmosphere (reaction 6, Table 4). The arrows and letter annotations at the top of the diagram refer to sequential events in reaction progress (see Figs. 2c, 28, and 29).

gress; *i.e.*, continued reaction causes the fugacity of O_2 to increase, and chalcopyrite, biotite and quartz then coprecipitate at the expense of magnetite, K-felsdpar and albite. A second generation of chalcopyrite thus results from the reaction. Eventually the solution becomes saturated with montmorillonite, and at a later stage with sphalerite. Sphalerite and magnetite then replace chalcopyrite until all the chalcopyrite is destroyed. At this point biotite and sphalerite begin replacing magnetite, which continues until all the magnetite is consumed. Further reaction results in precipitation of sphalerite, biotite, montmorillonite, and quartz until the solution equilibrates with albite and K-feldspar (Figures 30 and 31). In summary, the sequence of events involving magnetite and the sulfide minerals is: (1) precipitation of pyrite, (2) replacement of pyrite by magnetite, (3) replacement of pyrite by chalcopyrite and magnetite, (4) cotectic precipitation of chalcopyrite and magnetite, (5) dissolution of magnetite and chalcopyrite, (6) replacement of magnetite by chalcopyrite, (7) replacement of chalcopyrite by magnetite and sphalerite, (8) replacement of magnetite by sphalerite, (9) precipitation of sphalerite. Note in Figure 31 that sphalerite is present throughout a large range of solution pH (3.75–5.7).

In the reaction illustrated in Figures 30 and 31, the mass of chalcopyrite precipitated from solution (and subsequently destroyed) constitutes 1.5 percent copper ore, based on the mass of quartz produced (kgm H_2O)$^{-1}$. The

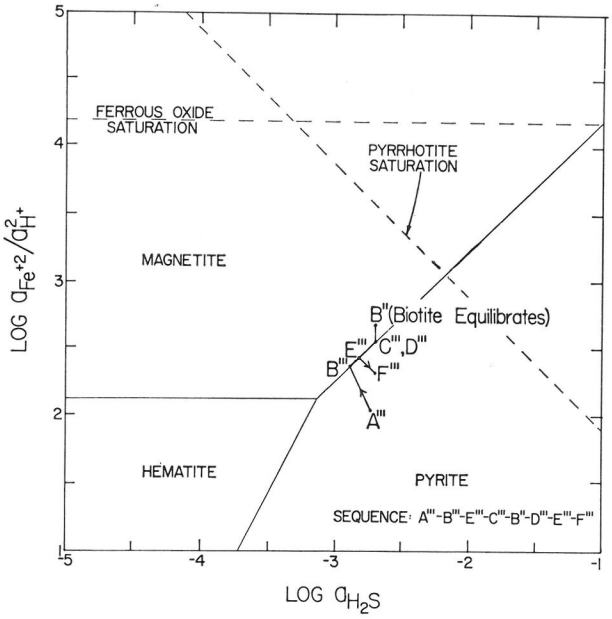

FIG. 28. Theoretical activity diagram for the system $FeCl_2$-HCl-H_2S-H_2SO_4-H_2O in the presence of an aqueous phase at 300°C, one atmosphere, and unit activity of H_2O. The arrows and letter annotations refer to the reaction depicted in Figs. 2c, 27, and 29 (reaction 6, Table 4).

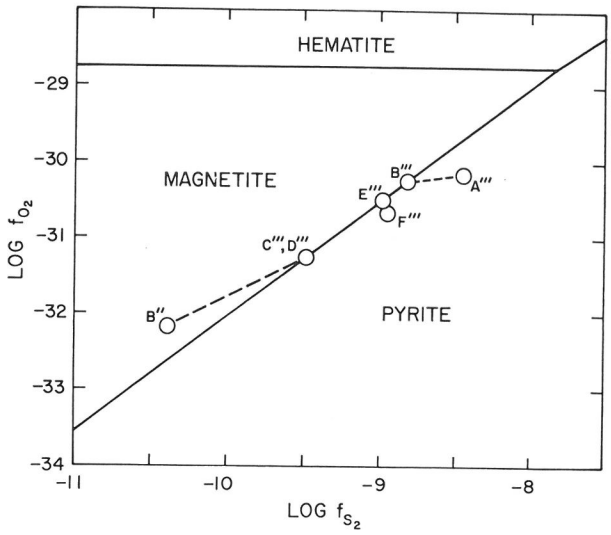

FIG. 29. Theoretical fugacity diagram for the system Fe-S-O at 300°C and one atmosphere (based on thermodynamic data summarized by Helgeson, 1969). The dashed lines and letter annotations refer to the reaction depicted in Figs. 2c, 27, and 28 (reaction 6, Table 4).

mass of sphalerite precipitated corresponds to ~5 percent zinc ore on the same basis. The overall reaction causes a net increase in solution of the concentrations of aluminum (from 3 to 180 ppm), potassium (from 388 to 465 ppm), and sodium (from 1,140 to 1,370 ppm), and a decrease in the concentrations of iron (from 55 to 4 ppm), zinc (from 649 to 591 ppm), sulfide (from 40 to 15 ppm) and sulfate (from 12 to 11 ppm). In the process, more than 14 ppm copper are removed and subsequently returned to the aqueous phase.

Comparison of mass transfer at 100°, 200°, and 300°C. It can be concluded from the mass transfer calculations summarized above that precipitation of a chalcopyrite-sphalerite orebody from acid alkali-chloride solutions at 300°C requires either a very low concentration of chloride in solution, or very large concentrations (tens of thousands of ppm) of copper and zinc or sulfide and sulfate. The stabilities of chloride complexes involving copper and zinc

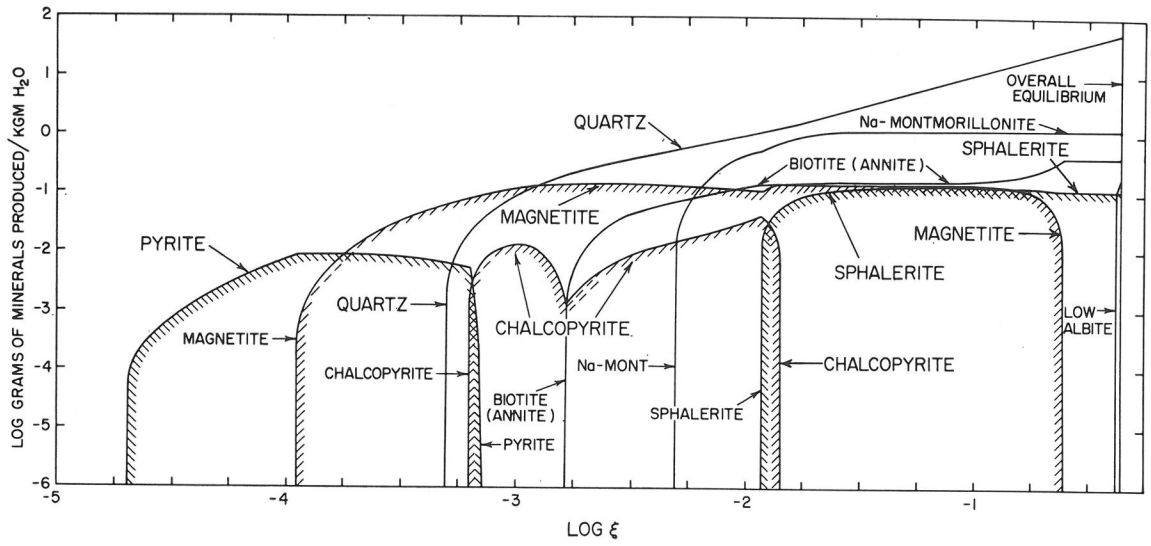

FIG. 30. Mass of minerals produced (kgm H_2O)$^{-1}$ as a function of progress in the reaction of a dilute acid hydrothermal solution with an hypothetical quartz+microcline+albite+annite rock at 300°C and one atmosphere (reaction 7, Table 4—see Fig. 31).

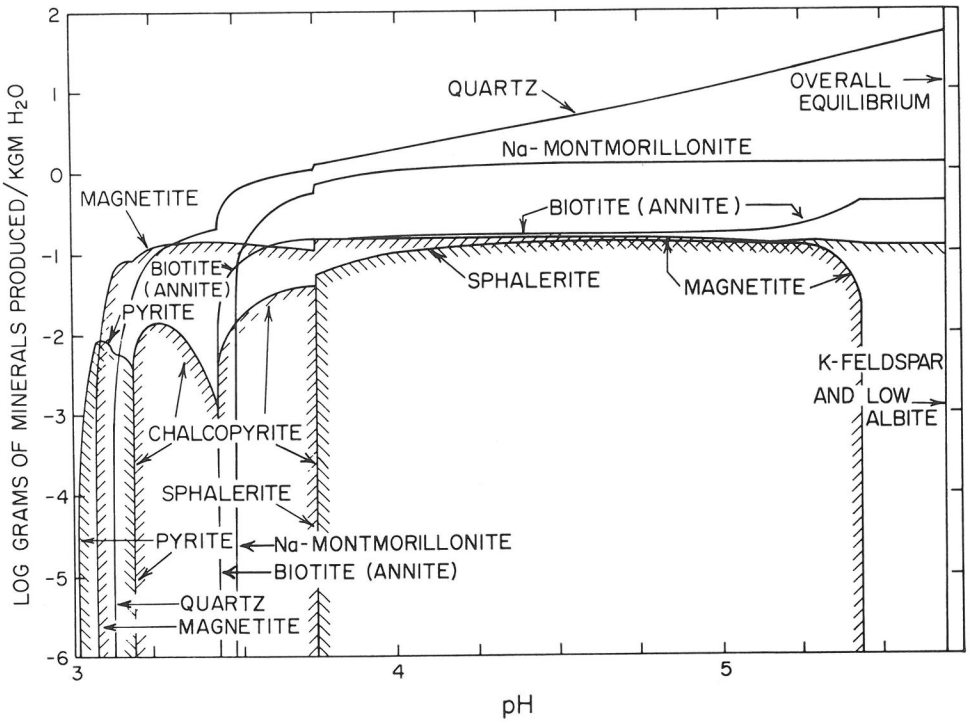

FIG. 31. Mass of minerals produced (kgm H_2O)$^{-1}$ as a function of solution pH in the reaction depicted in Figure 30 (reaction 7, Table 4).

and the solubilities of their sulfides in chloride-rich solutions are substantially higher at 300°C than they are at lower temperatures (Helgeson, 1969).

Comparison of the mass of the various sulfides produced (kgm H_2O)$^{-1}$ in reactions 1, 4, and 6 (Table 4) at 200°, 100°, and 300°C, respectively, can be made in Figures 32 and 33.

The results of the calculations are presented in Figure 32 in the form of paragenesis diagrams at the three temperatures, and in Figure 33 as a function of temperature. It can be seen in these figures that a change of 100° in temperature causes a change in mass transfer of about 2 orders of magnitude.

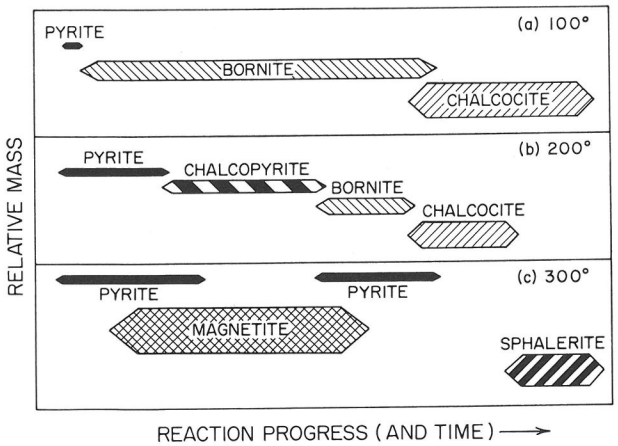

FIG. 32. Comparative paragenesis diagrams depicting the relative mass of pyrite, bornite, chalcopyrite, magnetite, and sphalerite precipitated as a function of progress in the reaction of acid chloride-rich hydrothermal solutions with an hypothetical quartz +microcline+albite+annite rock at 100°C (diagram a—reaction 4, Table 4 and Figs. 2a and 23), 200°C (diagram b—reaction 1, Table 4 and Figs. 2d and 11–15), and 300°C (diagram c—reaction 6, Table 4 and Figs. 2c and 27–29).

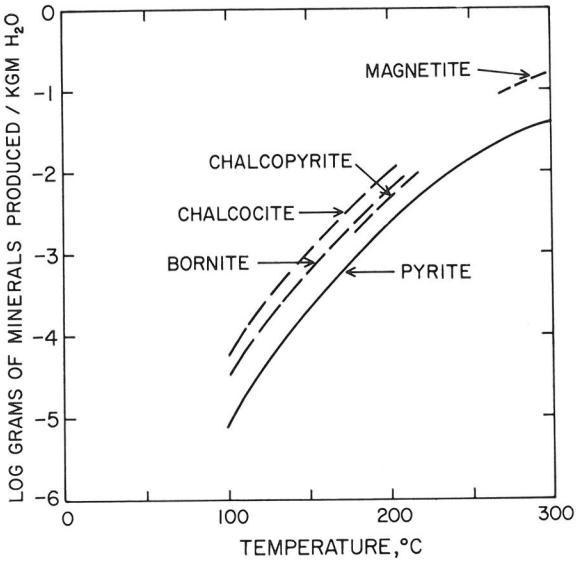

FIG. 33. Mass of minerals produced and destroyed (kgm H_2O)$^{-1}$ in reactions 1, 4, and 6 (Table 4 and Figs. 2a, c, and d, 11–15, 23, and 27–29).

Reactions with Limestone at 150°C (Mississippi Valley Type Ore Deposition)

Reactions between acid alkali-chloride hydrothermal solutions and limestone at 150°C (reactions 8–12, Table 4) are illustrated in Figures 34–40.

Reactions involving dilute alkali-chloride solutions. Reaction of a relatively dilute sodium-magnesium-chloride solution (11190 ppm chloride) with limestone at 150°C (reaction 8, Table 4) leads to the redistribution of components illustrated in Figures 34–36. It can be seen in Figures 34 and 35 that the pH increase accompanying the initial congruent dissolution of calcite causes the solution to become saturated first with chalcocite at A, but continued reaction results in the appearance of bornite at B; bornite then replaces the earlier formed chalcocite along BC until all the chalcocite is consumed at C. As calcite continues to dissolve, bornite precipitates along CD, and at D galena becomes a reaction product. Galena and bornite then continue to precipitate until the solution becomes saturated with sphalerite at E. Further reaction results in replacement of bornite by sphalerite and minor precipitation of galena along EF. At F the solution becomes saturated (once again) with chalcocite, and almost immediately thereafter with magnetite at G. Along GH chalcocite, magnetite, and sphalerite replace bornite until all the bornite is consumed at H. Continued reaction causes coprecipitation of magnetite, chalcocite, sphalerite, and galena until the solution becomes saturated with dolomite at I. Dolomite then precipitates and the earlier formed minerals dissolve slightly until overall equilibrium is achieved at J.

It can be seen in Figures 35 and 36 that the appearance of dolomite causes a *p*H reversal as a function of reaction progress. The pH decrease from I to J is caused by the reaction

$$CaCO_3 + H_2CO_3 + Mg^{2+} \rightarrow CaMg(CO_3)_2 + 2H^+ \qquad (13)$$

Magnetite, chalcocite, sphalerite, and galena respond to the decreasing pH by dissolving in the final stage of reaction progress. Destruction of calcite reaches 1.5 grams (kgm H_2O)$^{-1}$ over reaction path ABCDEFGHIJ in Figures 35–37; 1.3 grams of dolomite (kgm H_2O)$^{-1}$ are precipitated in the interval IJ. Taking into account molar volumes (Robie and Waldbaum, 1968), these figures mean that the extent to which dolomite replaces calcite in the above reactions is about 20 percent less than the volume of calcite dissolved. The mass of sulfides precipitated (kgm H_2O)$^{-1}$ amount to slightly more than 0.1 percent of the mass of calcite destroyed (kgm H_2O)$^{-1}$. Over the whole reaction

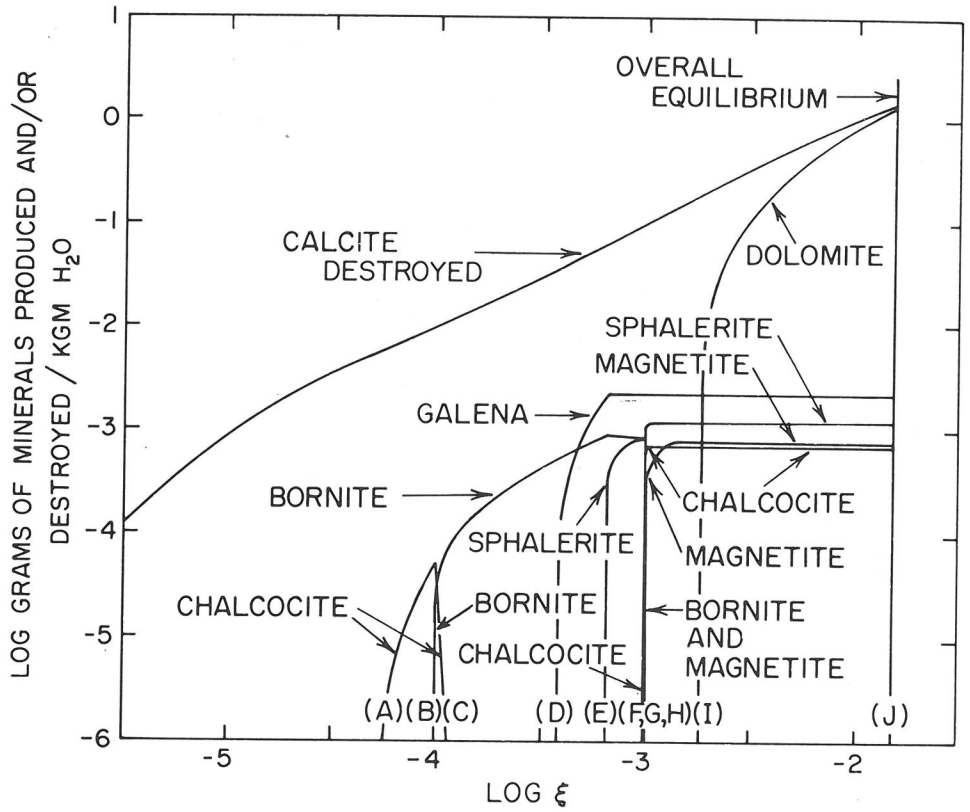

Fig. 34. Mass of minerals produced and destroyed as function of progress in the reaction of an hypothetical limestone with a dilute acid sulfide (and sulfate)-rich hydrothermal solution at 150°C and one atmosphere (reaction 8, Table 4). The letter annotations refer to sequential events in reaction progress (see Figs. 35 and 36).

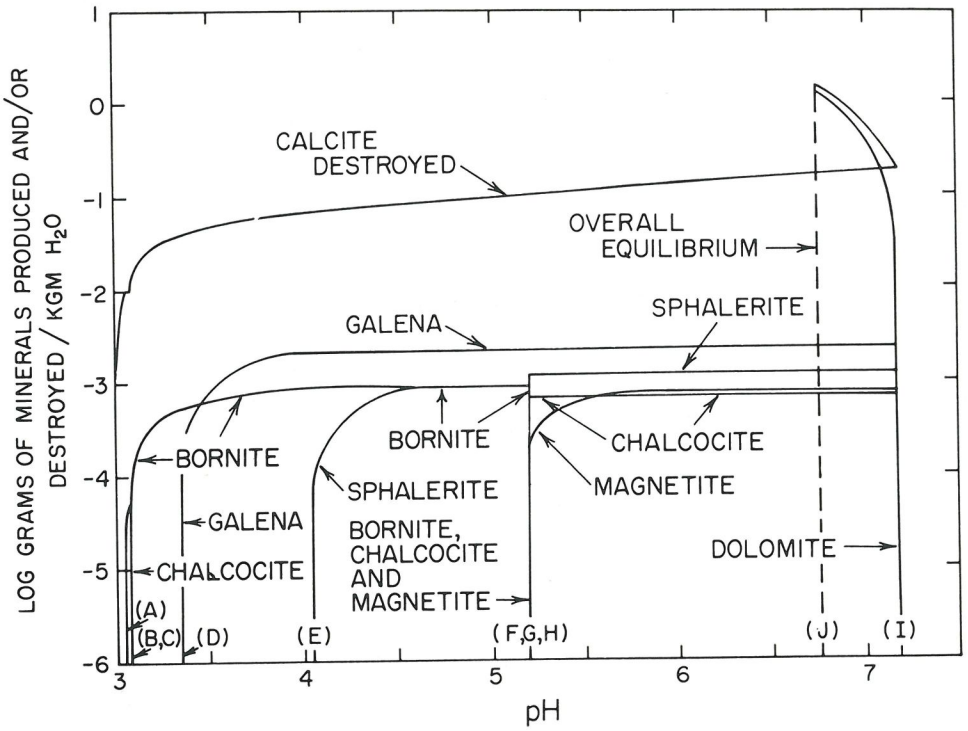

FIG. 35. Mass of minerals produced and destroyed (kgm H_2O)$^{-1}$ as a function of solution pH in the reaction depicted in Figs. 34 and 36 (reaction 8, Table 4). The letter annotations refer to sequential events in reaction progress.

path the fugacities of O_2 and S_2 decrease from 10^{-44} and 10^{-13} to 10^{-45} and 10^{-26}, respectively, while that of CO_2 increases from 10^{-5} to about a tenth of an atmosphere. Because the reaction coefficients of the sulfides and magnetite in the interval IJ are small, little change in the total molalities of lead, zinc, iron, copper, and sulfide occur along this segment of the reaction path. The changes in the molalities of HS^-, H_2S, HCO_3^-, Fe^{2+}, and $FeOH^+$ in the interval IJ in Figure 36 are caused by the redistribution of species resulting from the decrease in solution pH. Note that the chemistry of the aqueous phase changes drastically after the appearance of sphalerite (at E) and before the appearance of dolomite (at I), and that all the events at F, G, and H take place at essentially the same solution pH (Figure 36).

As noted above, two generations of chalcocite are produced along reaction path ABCDEFGHIJ in Figures 34–36. The reappearance of chalcocite (in the interval FGHIJ) at a later stage of reaction progress (after early precipitation of chalcocite in the interval AB, and subsequent replacement of chalcocite by bornite in the interval BC) is a consequence of the greater increase in the activity of S^{2-} compared to the decrease in the activity of Cu^+ in the interval CF. Such behavior is probably typical of hydrothermal systems involving sulfide deficient solutions; *i.e.*, many such systems would be expected to exhibit multiple generations of sulfides.

The effect of a higher initial oxidation state on the reaction discussed above can be assessed in Figure 37. The composition of the aqueous phase involved in this reaction (reaction 9, Table 4) is identical to that in the reaction represented in Figures 34–36 (reaction 8, Table 4), except for the intial concentration of sulfate (15 ppm compared to 0.3 ppm). The higher concentration of sulfate causes an initial fugacity of O_2 of $10^{-43.4}$ compared to $10^{-44.2}$ in the previous case. Although the complete reaction is not depicted in Figure 37, it can be seen that the slightly higher oxidation state of the initial solution prevents precipitation of chalcocite, and causes hematite to appear as a reaction product instead of magnetite. The paragenetic sequence in Figure 37 is: (1) bornite, (2) bornite + galena, (3) sphalerite + bornite + galena, and (4) hematite + bornite + sphalerite + galena. This sequence, although incomplete, is considerably different from that produced in the preceding case; *i.e.*, (1) chalcocite, (2) chalcocite + bornite, (3) bornite, (4) bornite + galena, (5) bornite + sphalerite + galena, (6) bornite + sphalerite + galena + chalcocite, (7) bornite + sphalerite + galena + chalcocite + magnetite, and (8) sphalerite + galena + chalcocite + magnetite.

Reaction involving a concentrated alkali-chloride solution. The mass transfer resulting from reaction of a limestone with an acid hydrothermal solution containing 105,000 ppm sodium chloride (reaction 10, Table 4) is depicted in Figure 38. Although the complete reaction is not rep-

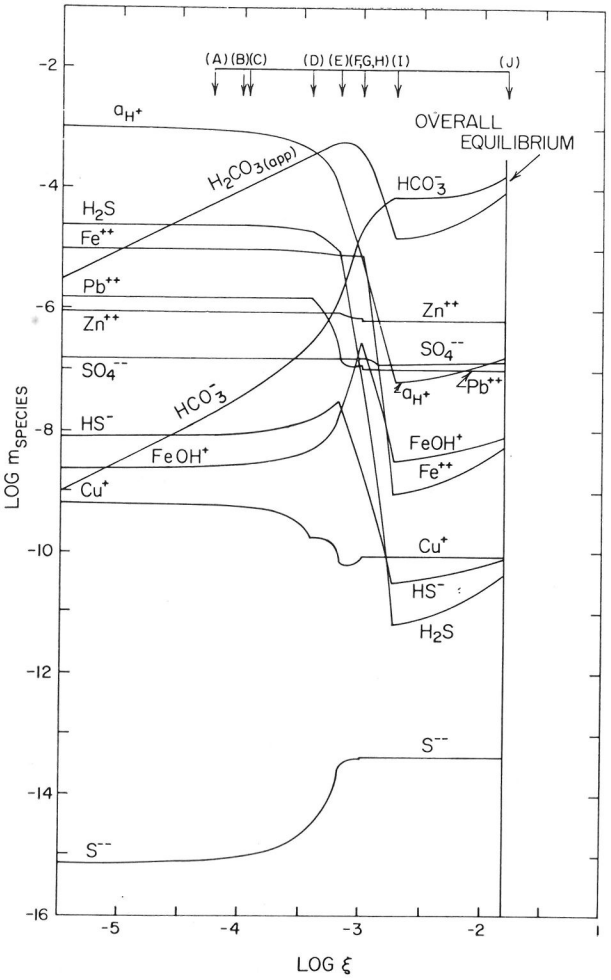

FIG. 36. Molalities of species in an aqueous phase reacting with limestone at 150°C (reaction 8, Table 4). The arrows and letter annotations refer to sequential events in reaction progress (see Figs. 34 and 35).

resented in Figure 38, it can be deduced from comparison of Figures 35, 37, and 38 that the higher concentration of chloride affects considerably the consequences of reaction progress. As observed above, the higher chloride concentration increases the ability of the solution to transport metal ions as chloride complexes (Helgeson, 1969). In this case (Figure 38) the initial solution contains 1 ppm iron, 18 ppm lead, 29 ppm zinc, 6 ppm copper, 3 ppm sulfive, and 9 ppm sulfate, with an initial pH of 3.0. Reaction of the solution with calcite at 150°C leads first to the appearance of pyrite, which precipitates until the solution becomes saturated with galena. As calcite continues to dissolve, galena replaces the earlier-formed pyrite; however, before all the pyrite is consumed, the solution becomes saturated with bornite, which then joins galena in replacing pyrite. After destruction of all the pyrite, bornite coprecipitates with galena, but then it soon begins to dissolve slightly. With further reaction progress, the solution becomes saturated with magnetite, and magnetite and galena then precipitate at the expense of bornite and calcite.

The mass of galena precipitated in the reaction depicted in Figure 38 is about 20 percent of the mass of calcite dissolved, compared to 2 percent at a comparable stage of progress in reaction 8 (Figure 35). Note that the mass ratio of galena to bornite in Figure 35 is 2.5, while that in Figure 38 is greater than 7. There can be little doubt that the reaction represented in Figure 38 is capable of causing deposition of sulfides in ore proportions. Reaction up to the point represented by the right side of Figure 38 causes abstraction of 15 ppm lead and 1 ppm copper from the aqueous phase.

Reactions without replacement. Mississippi Valley ore deposits exhibit little or no replacement of sulfides. On the other hand, they are characterized by multiple generations of sulfides precipitated in open spaces. The depositional process responsible for these phenomena can be modeled by carrying out calculations similar to those described above, but with the stipulation that earlier-formed minerals do not react with the solution at later stages of reaction progress.[1] Model calculations for such a system are illustrated in Figures 39 and 40 for reaction of a limestone with a dilute (reaction 11, Table 4 and Figure 39) and concentrated (reaction 12, Table 4 and Figure 40) sodium chloride

[1] In the actual case, such reactions may be precluded by the flow characteristics of the aqueous phase.

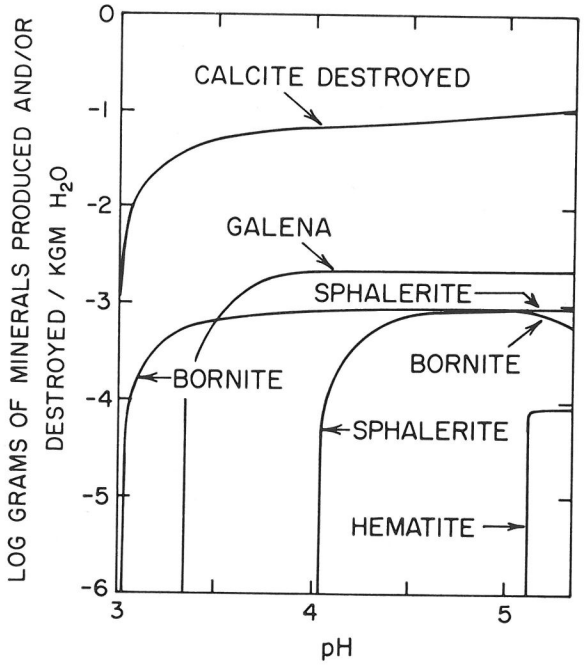

FIG. 37. Mass of minerals produced and destroyed as a function of solution pH during reaction of a dilute acid sulfide (and sulfate)-deficient hydrothermal solution with an hypothetical limestone at 150°C and one atmosphere (reaction 9, Table 4). Only the first part of the reaction is depicted in the diagram.

solution containing small concentrations of other components. To facilitate comparison of mass transfer, the same initial solution composition was used in reactions 8 and 11, and 10 and 12 (Table 4), respectively. Figures 35 and 39, and Figures 38 and 40 thus depict the consequences of identical reactions, except that earlier-formed minerals were not permitted to react with the aqueous phase at later stages of reaction progress in Figures 39 and 40.

It can be seen by comparing Figures 35 and 39 that preventing reaction of earlier-formed phases with the dilute solution precludes the appearance of second generation chalcocite. Also, there is no increase in the mass of sphalerite precipitated, and bornite is preserved rather than destroyed. In summary, the paragenesis illustrated in Figure 39 is: (1) chalcocite, (2) bornite, (3) bornite + galena, (4) galena + sphalerite, and (5) galena + sphalerite + magnetite.

In contrast to the dilute case, the constraint imposed on the reaction in Figure 40 causes a substantial decrease in the mass of bornite produced (kgm $H_2O)^{-1}$. The mass of bornite produced by the reaction in Figure 38 is about an order of magnitude higher than that produced by the reaction in Figure 40, owing to the fact that in the latter case the earlier-formed pyrite was not permitted to go into solution in later stages of reaction progress. The paragenesis in Figure 40 is: (1) pyrite, (2) galena, (3) galena + bornite, (4) galena, and (5) galena + magnetite. In contrast, the paragenesis in Figure 38 is: (1) pyrite, (2) pyrite + galena, (3) pyrite + galena + bornite, (4) galena + bornite, and (5) galena + bornite + magnetite. It can be seen in Figure 40 that the mass of galena and dolomite

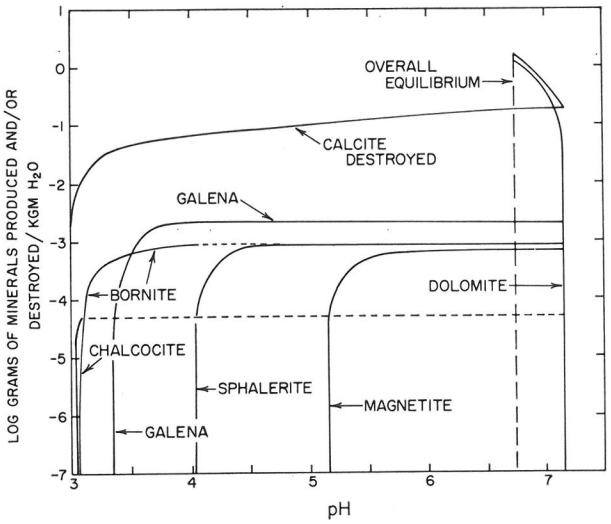

FIG. 39. Mass of minerals produced and destroyed as a function of pH during reaction of a dilute acid hydrothermal solution with an hypothetical limestone at 150°C and one atmosphere (reaction 11, Table 4) in a system in which minerals produced by the reaction cannot react with the aqueous phase at later stages of reaction progress. Precipitation of minerals (and dissolution of calcite) is represented by solid lines, and the preservation of earlier formed minerals by dashed lines. The dashed lines thus indicate intervals of reaction progress in which the aqueous phase is undersaturated with respect to the mineral.

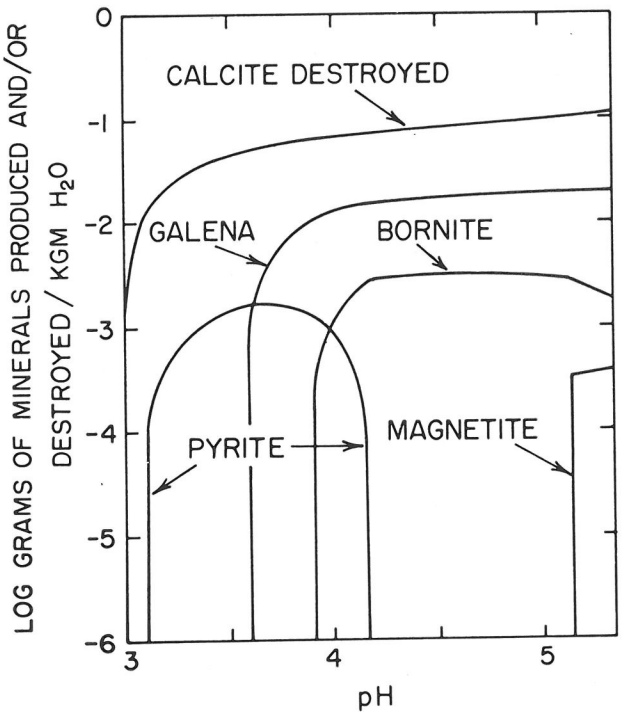

FIG. 38. Mass of minerals produced and destroyed as a function of solution pH during reaction of an acid chloride-rich hydrothermal solution with an hypothetical limestone at 150°C and one atmosphere (reaction 10, Table 4). Only the first part of the reaction is depicted in the diagram.

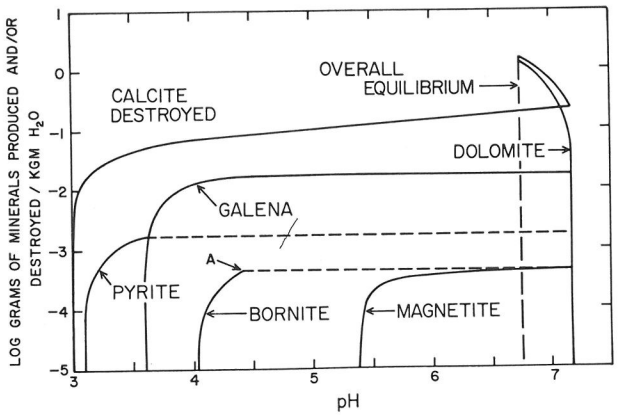

FIG. 40. Mass of minerals produced and destroyed as a function of pH during reaction of an acid chloride-rich hydrothermal solution with an hypothetical limestone at 150°C and one atmosphere (reaction 12, Table 4) in a system in which minerals produced by the reaction cannot react at later stages of reaction progress. Precipitation of minerals (and dissolution of calcite) is represented by solid lines, and the preservation of earlier formed minerals by dashed lines. The dashed lines thus indicate intervals of reaction progress in which the aqueous phase is undersaturated with respect to the mineral.

precipitated (kgm H_2O)$^{-1}$ is equal to about 1 percent and 80 percent, respectively, of the mass of calcite destroyed at the end of the reaction process. As before, the appearance of dolomite causes the solution pH to decrease with continued reaction progress. As in all of the limestone cases (Table 4), the overall reaction leads to an appreciable increase in the amount of open space in the reactant rock.

Minerals and Solution Chemistry

It has long been recognized that the presence of one or another mineral in a vein system may affect considerably the chemistry of hydrothermal processes. Mass transfer calculations define quantitatively the roles played by these minerals.

The appearance of calcite as a reaction product imposes a constant solution pH on continued reaction progress if the concentrations of Ca^{2+} and CO_2 in the aqueous phase are much higher than the change in the concentrations of these species resulting from reaction of the solution with its environment. If this constraint is established when two sulfides are precipitating, it may cause one of the two to replace the other as the solution continues to react with minerals in the host rock. Only after the concentration of Ca^{2+} or CO_2 begins to change can the pH again increase with continued reaction progress. Thus the early appearance of calcite may have a profound effect on the chemistry of subsequent hydrothermal reactions.

Pyritization of wall rocks, which is accompanied by oxidation of S^{2-} and reduction of SO_4^{2-} (as, for example, in $4KFe_3AlSi_3O_{10}(OH)_2+7H^++3HSO_4^-+21H_2S \rightarrow 2Al_2Si_2O_5(OH)_4+8SiO_2+4K^++12FeS_2+26H_2O$) serves to store sulfide for the formation of later copper-iron sulfides. Precipitation of biotite, chlorite, or siderite also affects considerably the chemistry of hydrothermal processes. The early appearance of one or more of these minerals promotes the appearance of copper-rich sulfides at later stages of reaction progress. Precipitation of magnetite or hematite may cause a drastic decrease in the fugacity of O_2 and either precipitation or dissolution of pyrite and copper-iron sulfides depending on the relative sizes of $\bar{n}_{Fe^{2+}}$, $m_{Fe^{2+}}$, $\bar{n}_{SO_4^{2-}}$, $m_{SO_4^{2-}}$, $\bar{n}_{S^{2-}}$, and $m_{S^{2-}}$. Precipitation of biotite may also destroy pyrite. If magnetite (or hematite) is present when other iron-bearing minerals such as biotite begin to form, the iron oxide may dissolve to provide iron for the new phase, thereby causing the fugacity of O_2 in the system to increase substantially. As this occurs, sulfides may precipitate from solution. As emphasized above, intermittent hydrothermal leaching and multiple generations of sulfides may be produced in this way.

Reaction of sulfate (and sulfide)-deficient solutions with limestone may also result in multiple generations of sulfides. Hydrothermal leaching of minerals is promoted by decreasing solution pH, which occurs in a limestone environment following the appearance of such minerals as dolomite or ankerite as reaction products. The concentration of magnesium in the aqueous phase, and the stage of reaction progress at which dolomite appears are important discriminant factors in the process.

Dolomitization is only one of several acid-producing processes in hydrothermal systems. Precipitation of other carbonates or silicates, oxides, and sulfides may also produce hydrogen ion. The chemistry of the process can be illustrated by expressions written in terms of H^+ and the predominant species in the aqueous phase. For example, equilibrium precipitation of pyrite, chalcopyrite, bornite, magnetite and hematite can be represented by

$$4Fe^{2+} + 7H_2S + HSO_4^- \rightleftharpoons 4FeS_2 + 4H_2O + 7H^+ \quad (14)$$

$$8CuCl_3^{2-} + 8Fe^{2+} + 15H_2S + HSO_4^- \rightleftharpoons 8CuFeS_2 + 4H_2O + 24Cl^- + 23H^+ \quad (15)$$

$$40CuCl_3^{2-} + 8Fe^{2+} + 31H_2S + HSO_4^- \rightleftharpoons 8Cu_5FeS_4 + 4H_2O + 120Cl^- + 55H^+ \quad (16)$$

$$12Fe^{2+} + 12H_2O + HSO_4^- \rightleftharpoons 4Fe_3O_4 + H_2S + 23H^+ \quad (17)$$

$$8Fe^{2+} + 8H_2O + HSO_4^- \rightleftharpoons 4Fe_2O_3 + 15H^+ + H_2S \quad (18)$$

All of these reactions are displaced to the right by decreasing temperature and/or reaction of the aqueous phase with granitic or calcareous rocks. Congruent precipitation of sulfides in response to a decrease in temperature may thus increase the reactivity of a hydrothermal solution with respect to its environment. Precipitation of iron sulfides or oxides, and copper or copper-iron sulfides may be accompanied by an overall increase or decrease in the fugacity of O_2 in the system, depending on the relative sizes of the reaction coefficients and the concentrations of SO_4^{2-} and S^{2-} in solution.

As indicated above, mass transfer calculations suggest that deposition of silver, lead, zinc, copper, and copper-iron sulfides in ore proportions from acid alkali-chloride solutions at high temperatures (300°C and above) requires either relatively dilute aqueous chloride solutions or relatively high concentrations (tens of thousands of ppm) of the ore-forming metals or sulfide and sulfate in solution. The high solubilities of both aluminosilicates and sulfides in acid chloride-rich solutions at high temperatures favors metasomatic alteration of rocks and hydrothermal transport (rather than deposition) of sulfides. Adiabatic expansion of such a solution may cause precipitation of sulfides in ore proportions (Helgeson, 1964). However, preliminary theoretical calculations suggest that *mass transfer as a function of temperature and/or pressure is not equivalent quantitatively to mass transfer in response to isothermal reaction of solution with its mineralogic environment.*

Discussion

The presence of large masses of anhydrite in an ore deposit suggests precipitation of sulfides from solutions containing low concentrations of calcium and high concentrations of sulfate and sulfide (of the order of thousands or tens of thousands of ppm at temperatures greater than 250°C). In general, the activity of the sulfate ion in solution (and thus the tendency to precipitate anhydrite in response to increasing activity of the sulfate ion) is insensitive to changes in solution pH from 3 to ~6. This observation is underscored by the fact that the aqueous phase was nearly saturated with anhydrite at the outset of several of the reactions discussed above, but anhydrite

failed to appear as a reaction product. It is important to note in this regard that the solutions involved in the reactions all contained substantial concentrations of the calcium ion relative to the mass transfer of the calcium ion from the reactant rock to the aqueous phase. The solubilities of anhydrite, calcite, and nonaluminous ferromagnesian silicates decrease with increasing temperature, which no doubt affects considerably their occurrence in hydrothermal systems. However, where the activity of Ca^{2+} in the initial solution is low and the concentration of sulfate high, isothermal reaction of the solution with plagioclase may cause precipitation of anhydrite. An increase in the fugacity of O_2 should then accompany increasing solution pH as the reaction progresses, which favors deposition of sulfides. Precipitation of a more sodium-rich plagioclase (than that in the original rock) or a sodium-rich montmorillonite as a reaction product would be consistent with isothermal precipitation of anhydrite from sulfide (and sulfate)-rich calcium-poor solutions.

The relative mass of sulfides produced (kgm $H_2O)^{-1}$ as a function of reaction progress in the model calculations discussed above is generally consistent with volume for volume replacement of precursing minerals; *i.e.*, the mass of a sulfide precipitated at the expense of an earlier sulfide is usually greater than the mass of the mineral dissolved. In contrast, sulfide replacement of carbonates leads to a large increase in open space. The mass transfer calculations suggest that the classical Butte pattern of silicate alteration and sulfide zoning may form (at least in part) at temperatures well below 200°C, and that only a small fraction of the ore-forming metals and/or sulfide in hydrothermal solutions may be extracted to form an ore deposit (with the remainder passing out of the system to be lost eventually through dilution of the hydrothermal solution with ground water). On the other hand, the concentrations of sulfide and/or the ore-forming metals in solution may have been considerably lower than those generally considered "reasonable" (*i.e.*, lower than part per million concentrations). The large volumes of fluid required to form ore deposits from such solutions are consistent with those needed to account for the metasomatic features and isotopic compositions of the minerals in the marginal zones of large igneous intrusives (Taylor and Epstein, 1968).

Convective models of solution flow such as that suggested by Taylor and Epstein (1968) and Sheppard, Nielsen, and Taylor (1969) in the vicinity of a hot intrusive body are consistent with the zonal pattern of sulfides and alteration minerals observed in porphyry copper deposits. An aqueous phase entering the high temperature environment at depth, where the solubilities of aluminosilicates and sulfides are high, should react aggressively with the intrusive and derive material from the host rock. As the solution rises along the margins of the intrusive and the temperature decreases, sulfides may precipitate, thereby lowering the solution pH and promoting further reaction of the solution with silicates at shallow depths. Aluminosilicates may also precipitate as the aqueous phase rises through the contact zone of the intrusive; in contrast, ferromagnesian silicates tend to dissolve as temperature decreases. The pressure distribution in the system should cause the solutions to permeate through fractures from the margins toward the center of the crystallized (but still hot) intrusive, leaving a pattern of mineralization consistent with increasing temperature, diminishing acid attack, and increasing approach to equilibrium from the outside toward the center. This is the gross pattern observed in porphyry copper deposits; *i.e.*, the outer zones are characterized by the occurrence of pyrite and sericite, and the inner zones by chalcopyrite, and secondary biotite and K-feldspar. Solution flow from the margins toward the center of a district also fits the zonal distribution of mineralization at Bingham, Butte, and other hydrothermal base metal deposits. Horizontal temperature gradients probably play minor roles in the depositional process, which may take place at both high and/or low temperatures. In most instances the source of the aqueous phase is probably the surrounding sediments; however, the ore-forming metals may be derived either from the sediments (Helgeson, 1967b) or the intrusive at depth.

Concluding Remarks

The hydrothermal systems considered in the preceding pages are only a few of many that deserve similar investigation; *e.g.*, sufficient data are available to study gold, silver, mercury, tin, native copper, and arsenic deposition in the same way. However, comprehensive calculations will require more experimental information (such as the thermodynamic properties of enargite, tennantite, tetrahedrite, etc.) and extensive use of high speed digital computers with large storage capacities. The effects of different initial concentrations of aqueous species on mass transfer have yet to be determined for a number of components. The chemical consequences of the presence and compositional variability of phases containing Fe^{3+}, Fe^{2+}, and Mg^{2+} such as chlorite, epidote, and biotite, as well as siderite, ankerite, anhydrite, arsenopyrite, muscovite, montmorillonite, and other minerals in hydrothermal systems need to be explored in greater detail. As in the case of enargite, such studies will require more and better thermodynamic data. The importance of this observation is underscored by the fact that thermodynamic data presently available require montmorillonite to be considerably more stable than K-mica in hydrothermal systems (Helgeson, 1969). The abundance of sericite in hydrothermal ore deposits suggests that the enthalpy of formation from the elements of K-mica is actually several kilocalories more negative than that presently in use. Similarly, the stability constants for aluminum hydroxide complexes at elevated temperatures are probably smaller than those used in this study (Helgeson, 1970b), which means the solubilities of aluminosilicates at high temperatures should be lower than those predicted above. More experimental calorimetry is required to resolve such uncertainties. Additional thermodynamic data will also permit comprehensive mass transfer calculations to be carried out for simultaneous changes in temperature, pressure, and reaction progress. Ultimately it should

be possible to include explicit and simultaneous provision in mass transfer calculations for diffusional constraints, convection, fluid flow, metastable equilibria, and selective supersaturation of minerals in the aqeuous phase.

If mass transfer calculations are correlated closely with geologic reality, quantitative field observations can be used to derive realistic theoretical models of geochemical processes. In principle, mass transfer calculations represent a potential tool of ore search. Repeated and sequential cyclic interchange of theoretical predictions and field observations should lead to a converging series of approximations of the specific chemical environment responsible for the formation of a given ore deposit. The observations needed are: (1) *fluid inclusion analyses and temperatures of filling*, (2) *mineral compositions and compatibilities among the silicates, sulfides, oxides, carbonates, and sulfates*, (3) *quantitative information regarding zonal and paragenetic sequences and cotectic-peritectic relations*, (4) *the relative mass of each mineral in the system, and* (5) *the width of veins, directional evidence of solution flow, gains and losses in the alteration zones, etc.* Many discussions relating to such observations can be found in the geologic literature, but regrettably most of these are qualitative rather than quantitative.

The most important contributions to the understanding of ore transport and deposition are still to come from the field geologist. It is he who must supply the quantitative information needed for realistic derivation and evaluation of chemical and thermodynamic models of ore transport and deposition, and it is he who must apply the results of theoretical predictions to the geologic problem; therein lies the challenge for the modern geologist.

Acknowledgements

I am indebted to P. B. Barton, K. Krauskopf, G. Kullerud, J. J. Hemley, P. L. Cloke and U. Petersen for their helpful suggestions and critical reviews of the manuscript, and to R. H. Leeper for his invaluable assistance with the computer calculations and diagrams presented above. The calculations required approximately fifty hours of CDC 6400 computer time, most of which was contributed by Northwestern University. Financial support received from the National Science Foundation (NSF Grant GA 11285) is also acknowledged with thanks.

References

Althaus, E., and W. Johannes (1969) Experimental metamorphism of NaCl-bearing aqueous solutions by reactions with silicates. *Amer. J. Sci.* **267,** 87–98.

Barton, P. B., Jr. (1959) The chemical environment or ore deposition and the problem of low temperature ore transport. *In* P. Abelson, ed., *Researches in Geochemistry* John Wiley and Sons, New York, 279–299.

De Donder, Th. (1920) *Leçons de Thermodynamique et de Chimie-Phisique.* Gauthier-Villars, Paris.

Ellis, A. J., and W. A. J. Mahon (1967) Natural hydrothermal systems and experimental hot-water/rock interactions (Part II). *Geochim. Cosmochim. Acta* **31,** 519–539.

Fisher, J. R. (1969) *The Ion Product of Water to 350°C.* Ph.D. dissertation, Department of Geochemistry and Mineralogy, The Pennsylvania State University.

Garrels, R. M., and C. L. Christ (1965) *Solutions, Minerals, and Equilibria*, Harper and Row, New York, 450 p.

Helgeson, H. C. (1964) *Complexing and Hydrothermal Ore Deposition.* Pergamon Press Inc., New York, 128p.

——— (1967a) Solution chemistry and metamorphism, *In* P. Abelson, ed., *Researches in Geochemistry, Vol. II*, John Wiley and Sons, New York, 362–404.

——— (1967b) Silicate metamorphism in sediments and the genesis of hydrothermal ore solutions. *Econ. Geology Mon.* **3,** 333–342.

——— (1968) Evaluation of irreversible reactions in geochemical processes involving minerals and aqueous solutions: I. Thermodynamic relations. *Geochim. Cosmochim. Acta* **32,** 853–877.

——— (1969) Thermodynamics of hydrothermal systems at elevated temperatures and pressures. *Amer. J. Sci.* **267,** 729–804.

——— (1970a) Description and interpretation of phase relations in geochemical processes involving aqueous solutious. *Amer. J. Sci.* **268,** 415–438.

——— (1970b) Kinetics of mass transfer among silicates and aqueous solutions. *Geochim. Cosmochim. Acta* (in press).

——— (1970c) Reaction rates in hydrothermal flow systems. *Econ. Geol.* **65,** 299–303.

———, T. H. Brown, and R. H. Leeper (1969) *Handbook of Theoretical Activity Diagrams Depicting Chemical Equilibria in Geologic Systems Involving Minerals and an Aqueous Phase at One Atm. and 0°—300°C.* Freeman, Cooper, and Co., San Francisco, 253 p.

———, ———, A. Nigrini, and T. A. Jones (1970) Calculation of mass transfer in geochemical processes involving aqueous solutions. *Geochim. Cosmochim. Acta* (in press).

———, and R. M. Garrels (1968) Hydrothermal transport and deposition of gold. *Econ. Geol.* **63,** 622–635.

———, R. M. Garrels, and F. T. Mackenzie (1969) Evaluation of irreversible reactions in geochemical processes involving minerals and aqueous solutions: II. Applications. *Geochim. Cosmochim. Acta* **33,** 455–481.

Hemley, J. J., and W. R. Jones (1964) Chemical aspects of hydrothermal alteration with emphasis on hydrogen metasomatism. *Econ. Geol.* **59,** 538–569.

———, P. B. Hostetler, A. J. Gude and W. T. Mountjoy (1969) Some stability relations of alunite. *Econ. Geol.* **64,** 599–612.

Meyer, C., and J. J. Hemley (1967) Wall rock alteration, *In* H. L. Barnes, ed. *Geochemistry of Hydrothermal Ore Deposits.* Holt, Rinehart, and Winston, Inc., New York, p. 166–235.

Prigogine, I., and R. Defay (1954) *Chemical Thermodynamics.* Longmans, Green and Co., New York. 543p.

Raymahashay, B. C., and H. D. Holland (1969) Redox reactions accompanying hydrothermal wall rock alteration. *Econ. Geol.* **64,** 291–305.

Robie, R. A., and D. R. Waldbaum (1968) Thermodynamic properties of minerals and related substances at 298.15°K (25.0°C) and one atomosphere (1.013 bars) pressure and at higher temperatures. *U. S. Geol. Surv. Bull.* **1259,** 256 p.

Roedder, E. (1967) Fluid inclusions as samples of ore fluids. *In* H. L. Barnes, ed. *Geochemistry of Hydrothermal Ore Deposits.* Holt, Rinehart, and Winston, Inc., New York, p. 515–567.

Sheppard, S. M. F., R. L. Nielsen, and H. P. Taylor, Jr. (1969) Oxygen and hydrogen isotope ratios of clay minerals from porphyry copper deposits. *Econ. Geol.* **64,** 755–777.

Taylor, H. P., Jr., and S. Epstein (1969) Hydrogen-isotope evidence for influx of meteoric ground water into shallow igneous intrusions (abstr.), *Geol. Soc. Amer. Spec. Pap.* **121,** 294.

Thompson, J. B., Jr. (1959) Local equilibrium in metasomatic processes. *In* P. Abelson, ed. *Researches in Geochemistry.* John Wiley and Sons, New York, 427–457.